Mineralogy and Petrology (2007) 90: 271–300
DOI 10.1007/s00710-006-0180-2
Printed in The Netherlands

Mineralogy and Petrology

Origin and evolution of topaz-bearing granites from the Nanling Range, South China: a geochemical and Sr–Nd–Hf isotopic study

J.-H. Yu[1,2], **S. Y. O'Reilly**[2], **L. Zhao**[1], **W. L. Griffin**[2], **M. Zhang**[2], **X. Zhou**[1], **S.-Y. Jiang**[1], **L.-J. Wang**[1], and **R.-C. Wang**[1]

[1] State Key Laboratory for Mineral Deposits Research, Department of Earth Sciences, Nanjing University, Nanjing, P.R. China
[2] GEMOC ARC National Key Centre, Department of Earth and Planetary Sciences, Macquarie University, Sydney, N.S.W., Australia

Received June 21, 2006; revised version accepted November 23, 2006
Published online February 20, 2007;
Editorial handling: J. Kosler

Summary

The F-rich Hongshan pluton in the eastern Nanling Range, southern China, is a topaz-bearing albite leucogranite. It is distinctive from other topaz-bearing felsic rocks in South China with respect to age, size, geochemical evolution and topaz mode and morphology. The Hongshan granites are highly peraluminous and characterized by high K_2O/Na_2O, Si, Rb, Cs, Nb, Ta and F, and low Ca, Ba, Sr, Zr, Hf, P, K/Rb, Zr/Hf and Eu/Eu*. The granites show significant trace-element variations with magma evolution, with increasing Rb, Cs, Nb, Ta, Sn, W and decreasing Sr, Ba, Zr, Hf, Y, REE, Pb, Th, K/Rb, Zr/Hf, Th/U and Eu/Eu*. These changes dominantly reflect fractional crystallization of plagioclase, biotite and accessory minerals such as zircon and monazite. The granites also exhibit a decrease in εNd(t = 225 Ma) from −7.9 to −11.7 with magma evolution. Modeling shows that the Nd isotopic variation could result from assimilation of the Taoxi Group wall rocks during fractional crystallization.

The Hongshan pluton also shows spatial geochemical variations; the most evolved parts are located in the southeastern part of the pluton, which would be the most likely target area for rare-metal mineralization commonly associated with other topaz-bearing granites.

Zircon grains from two rock types in the Hongshan body were analyzed *in situ* for U–Pb ages and Hf isotopic values. The concordant zircon grains mostly range from 218 to 230 Ma with an average of 224.6 ± 2.3 Ma (Indosinian). Some zircons with different internal structures and Hf isotope compositions, as well as monazite fragments, yield U–Pb ages of ca. 280 to 240 Ma, suggesting older thermal events in the studied area.

The εHf(t) of these older zircons is strongly negative (−12.3), implying a crustal source with a Paleoproterozoic model age, similar to that for the Proterozoic Zhoutan Group. The main (~225 Ma) zircon population exhibits less negative εHf(t) (−3.0 to −7.6) and Mesoproterozoic model ages, suggesting that the original magma of the Hongshan granite was generated from deeper Mesoproterozoic crust.

Introduction

Mesozoic granitic magmatism is abundant in southeastern (SE) China (Fig. 1) and commonly associated with valuable metal deposits. Based on their distribution, geochemical features, age and related mineralization type, two granite belts can be distinguished: one extends along the southeastern coastal region (Coastal belt) and the other over the Nanling Range (Nanling belt), respectively (Fig. 1b). The NE-oriented Coastal belt contains a large number of late Yanshanian (Cretaceous) granites and rhyolitic volcanic to subvolcanic rocks with minor early Yanshanian (Jurassic) rocks further inland. These felsic rocks are mostly calc-alkaline and high-K calc-alkaline in geochemistry, and commonly are associated with small amounts of contemporaneous gabbro or basalt and younger A-type granites. They are generally thought to have formed in a continental back-arc extensional setting, related to subduction of the Paleo-Pacific plate (*Lapierre* et al., 1997; *Xu* et al., 1999; *Zhou*

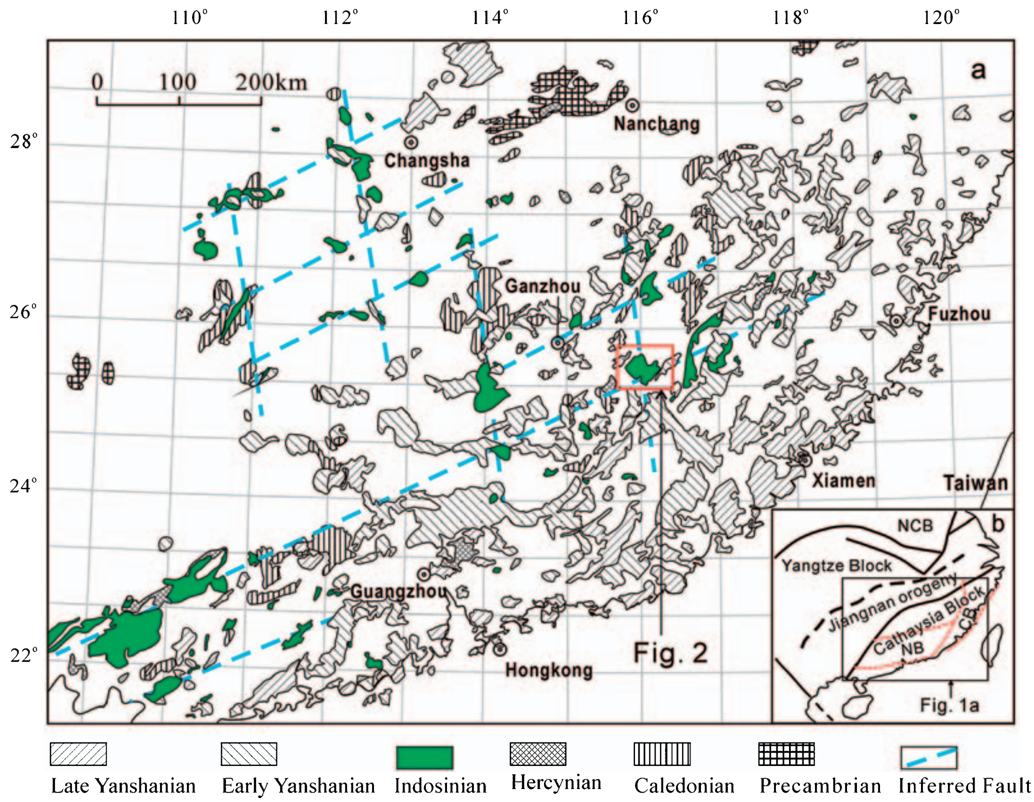

Fig. 1. Distribution of granites and location of the Hongshan pluton (**a**); and tectonic domains in SE China (**b**). *NCB* North China Block, *NB* Nanling belt, *CB* Coastal belt

and *Li*, 2000). The Nanling belt, which trends nearly E–W, is composed of large early Yanshanian granite bodies. Some Indosinian (Triassic) granites are scattered through this belt and nearby areas, but do not occur in the Coastal belt (Fig. 1). Early Yanshanian bimodal volcanic rocks and alkaline rocks have been found locally in the Nanling belt (*Li* et al., 2000, 2003; *Chen* et al., 1999, 2005). Relative to the Coastal belt, the Nanling belt contains more complex rock types with a wider range of ages. The tectonic setting of the Nanling granites and their relationship to the subduction of the Paleo-Pacific plate is still controversial (*Li* et al., 2000, 2003; *Zhou* and *Li*, 2000; *Zhou*, 2003; *Qiu* et al., 2005; *Sun* et al., 2005; *Ding* et al., 2006).

Topaz-bearing granitoids have been recognized in SE China in the past decade and have been referred to as topazite, ongonite, topaz-bearing sub-volcanic rocks, porphyries and albite granites (*Du* and *Huang*, 1984; *Zhu* et al., 1993; *Wang* et al., 1994; *Liu* and *He*, 1991, *Liu* et al., 1995, 1999). Such rock types also have attracted worldwide attention over the last two decades, not only because of their unique mineralogy and geochemistry, but also because they are commonly associated with rare-metal mineralization including W, Sn, Nb, Ta and U (e.g. *Christiansen* et al., 1983; *Taylor*, 1992; *Dostal* and *Chatterjee*, 1995; *Lenharo* et al., 2003; *Frindta* et al., 2004). The topaz-bearing felsic rocks in SE China generally have the following typical characteristics: 1) abundant topaz (usually $>$ 5 modal%) with >0.5 wt.% F in the bulk rock; 2) small outcrop areas (usually $<5\,km^2$); 3) shallow crystallization as sub-volcanic bodies or dykes, with a fine grained or porphyritic texture; 4) common association with rare-metal deposits; 5) multiple crystallization episodes of topaz, with idiomorphic, anhedral, and common acicular-prismatic grains; 6) highly evolved magma types; and 7) late Yanshanian (Late Mesozoic) ages (*Liu* and *He*, 1991; *Liu* et al., 1995, 1999; *Zhu* et al., 1993; *Wang* et al., 1994).

The Hongshan pluton was recently identified as one of the largest topaz-bearing granitic bodies in the Nanling belt (*Zhao* et al., 2004) and had been previously described as an andalusite-bearing peraluminous granite (*RGSTFJ*, 2000). It is very distinct from the other topaz-bearing felsic rocks in SE China in its occurrence at a deeper intrusive level, its texture, age and composition. The Hongshan pluton has not yet been explored for Sn, W, Nb and Ta mineralization. The aims of the present study are to define the petrogenesis of the Hongshan granite using detailed geochemical and geochronological data, and also to explore its potential for rare metal deposits.

Geological setting

The Hongshan granite is located in the eastern part of the Hongshan-Fucheng pluton (Fig. 2), which has an outcrop area of about $450\,km^2$ and was previously considered to be similar in lithology and age to the western part of the pluton (*RGSTJX*, 1991; *RGSTFJ*, 2000). However, our recent investigations indicate that the Hongshan-Fucheng pluton is a heterogeneous complex. It can be divided into at least three facies based on lithology: a fine- to medium-grained porphyritic topaz-bearing albite leucogranite that occurs in the eastern part (the Hongshan granite); a medium- to coarse-grained megacrystic biotite- to two-mica granite that occurs

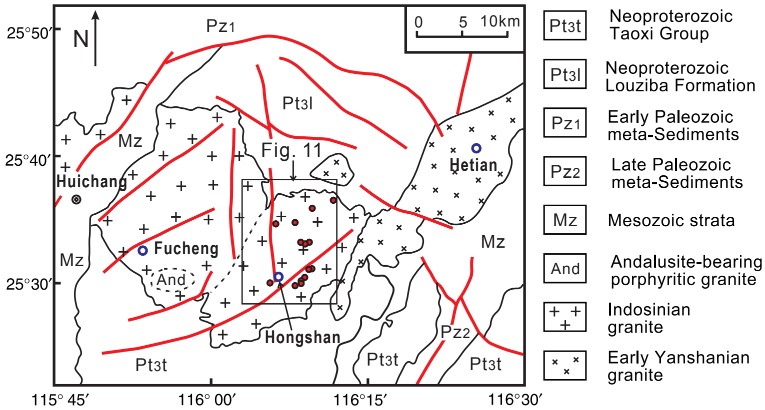

Fig. 2. Schematic geological map of the Hongshan-Fucheng granite complex

in the western part (the Fucheng granite); a fine-grained porphyritic andalusite-bearing granite outcropping within and intruding the Fucheng granite (Fig. 2). The contact relationships between the topaz-bearing granite and the biotite granite are unclear.

The Hongshan granite body shows intrusive contacts with the wall-rocks, including the Neoproterozoic Taoxi Group to the east and south, and the Sinian Louziba Formation to the north (Fig. 2). The western part is covered by the Cretaceous Ganzhou Formation, which is composed mainly of andesitic breccia, conglomerate, dark red sandstone, siltstone and mudstone, with a coarsening trend downward. The Taoxi Group consists of schists and gneisses mainly of amphibolite facies, but locally reaching granulite facies (*Yu* et al., 2003). The Louziba Formation consists of lower greenschist facies meta-greywacke, silts, marls and phyllites. The north-eastern part of the pluton was intruded by early Yanshanian coarse-grained garnet-bearing granite, implying that the Hongshan granite is older than Jurassic. Hence it was inferred to be formed in Triassic to Permian time (*RGSTFJ*, 2000).

Petrography

Fifteen samples were collected from the Hongshan pluton (Fig. 2). They are grey to pink, with a medium- to fine-grained seriate texture. K-feldspar is the most abundant phase in all samples, ranging from 35 to 45 vol.%. Perthitic K-feldspar occurs as megacrysts (or phenocrysts) of 1–4 cm in size, and represents 5–30 vol.% in different samples. The groundmass consists of K-feldspar, plagioclase and quartz with minor volatile-bearing minerals such as biotite, muscovite, topaz, fluorite and/or tourmaline. The sum of the feldspar and quartz modes exceeds 95 vol.%, so the Hongshan granite is classified as a leucogranite.

Plagioclase (20–30 vol.%) occurs generally as fine- to medium-grained euhedral crystals, commonly included in the coarse-grained or megacrystic K-feldspars, suggesting that they are an early-crystallizing phase. Quartz occurs as medium- to fine-grained anhedral crystals and may include fine-grained topaz.

Biotite makes up less than 3 vol.% and commonly is altered to muscovite or chlorite. Early biotite occurs as fine-grained subhedral grains or inclusions in feldspar. Later biotite occurs as both fine-grained anhedral and interstitial grains. Both primary and secondary muscovite has been distinguished in most rocks. Primary muscovite occurs interstitially as individual polygonal grains among euhedral feldspar. Secondary muscovite replaces biotite, topaz or feldspar.

Accessory minerals include topaz, tourmaline, zircon, monazite and apatite. Topaz is present in many Hongshan granite samples, and represents less than 2–3% by volume. It occurs typically as isolated fine-grained euhedral crystals or as fine-grained euhedral inclusions in quartz and feldspar. Tourmaline occurs in some samples, with euhedral prismatic morphology. Euhedral zircon and apatite are very fine-grained and quite sparse, especially in the highly evolved samples. Monazite occurs as two types: fine-grained (<0.2 mm) euhedral yellow grains and medium-grained (>0.3 mm) subhedral light yellow grains.

Analytical methods

Major- and trace-element analyses

Rock-forming mineral compositions were analyzed on a JXA8800 electron microprobe at the State Key Laboratory for Crust-Mantle evolution and Deposit Research, Nanjing University (China). An accelerating voltage of 15 kV, a beam current of 10^{-8} A and an electron beam of $\sim$1 μm were used for plagioclase, K-feldspar, biotite and muscovite analyses, while an accelerating voltage of 12 kV, a beam current of 10^{-8} A and an electron beam of 2 μm diameter were used for topaz analyses.

Major-element abundances of bulk rocks were determined by ARL9800XP^{+} X-ray fluorescence spectrometry at the Analysis Centre, Nanjing University. F contents were obtained using a TU-190 ultraviolet-visible light spectrophotometer at Nanjing Institute of Geology and Mineral Resources at room temperature and humidity of 46%. Trace-element analyses of bulk rocks were carried out using Finnigan MAT Element ICP-MS (inductively coupled plasma mass spectrometry) at Guiyang Institute of Geochemistry, Chinese Academy of Sciences. Standard AMH-1 and NBS-1663a were used to monitor the reliability of ICP-MS analytical results. The reproducibility by duplicated analysis of the standard for all elements was better than 10%. The analytical precision for most trace elements listed in Table 2 is better than 5%. Detailed analysis procedure is the same as described by *Qi* and *Grégoire* (2000).

Isotopic analyses

Ten samples with variable Rb/Sr ratio were chosen for Rb–Sr isotopic analyses, and a subset of five samples was chosen for Sm–Nd isotope analyses based on their Sm/Nd ratios. Powders crushed to less than 0.07 mm were dissolved in Teflon vials using standard dissolution procedures with HF and HNO_3. The dissolved sample was separated into two aliquots for analysis of element contents and isotopic analyses, respectively. Sm, Nd, Rb and Sr were separated using standard anion-exchange methods. Their contents were analyzed by isotope-dilution and Nd and Sr isotopic compositions were analyzed using a Finnigan MAT-261 thermal ionization mass spectrometer in the Isotope Laboratory at the Institute of Geology, Chinese Academy of Geological Sciences in Beijing. The $^{143}Nd/^{144}Nd$ and

$^{87}Sr/^{86}Sr$ ratios are normalized to $^{146}Nd/^{144}Nd = 0.7219$ and $^{86}Sr/^{88}Sr = 0.1194$. The measured $^{143}Nd/^{144}Nd$ ratio of the La Jolla standard is 0.511865 ± 12 (2σ, $n = 15$) and the measured $^{87}Sr/^{86}Sr$ ratio of the NBS987 standard is 0.71027 ± 12 (2σ, $n = 15$). The Nd and Sr procedural blanks in the laboratory are normally $<10^{-11}$ g and $<10^{-8}$ g, respectively.

U–Pb dating and Lu–Hf isotopic analyses of zircons were carried out at the GEMOC National Key Centre, Macquarie University, Sydney. Back scattered-electron/cathodoluminescence (BSE/CL) images were made for all analyzed zircons on a CAMECA SX100 electron microprobe to characterize the internal structure of the grains prior to U–Pb dating and Lu–Hf isotope analyses. U–Pb dating and Hf isotope analyses were performed using an HP 4500 series 300 ICP-MS and a Nu Plasma MC-ICP-MS, respectively, each fitted with New Wave Research LUV213 laser ablation microprobes. The detailed analytical conditions, procedures, correction methods and uncertainties are described by *Griffin* et al. (2002) and *Jackson* et al. (2004). The uncertainty of the ages reported in the text is 1-sigma.

Mineral chemistry

Electron-microprobe analyses show that plagioclase compositions in the Hongshan granites are quite homogeneous with low An (2.2–0.0%; Table 1), similar to those from other topaz-bearing granites (e.g. *Manning* and *Hill*, 1990; *Taylor*, 1992; *Kesraoui* and *Nedjari*, 2002). Therefore the Hongshan granites are topaz-bearing albite leucogranites. All matrix and megacryst K-feldspars have a high Or component (generally >96%; Table 1).

Biotite is rich in FeO (17.19–25.73 wt.%) and poor in MgO (1.46–2.83 wt.%) with low $Mg^{\#}$ (0.12–0.16), consistent with the highly evolved whole-rock compositions (see below). The primary white micas show large FeO and MgO variations, 2.4–10.0 wt.% and 0.42–1.5 wt.%, respectively, but homogeneous K_2O and Na_2O contents (Table 1). Previous studies indicate that white micas in topaz-bearing leucogranites commonly are Li-rich (*Taylor*, 1992; *Tischendorf* et al., 1997; *Kesraoui* and *Nedjari*, 2002). Although the Li_2O contents of these micas were not analyzed in this study, they can be approximately calculated using the empirical formula, $Li_2O = 2.7/(0.35 + MgO) - 0.13$ (*Tischendorf* et al., 1997), giving Li_2O contents of 1.3–3.4 wt.%, similar to those of white micas in most F-rich granitoid rocks (*Taylor*, 1992; *Manning* and *Hill*, 1990; *Xiong* et al., 2002). In the classification diagram of $Li–R^{3+} + Ti–R^{2+} + Mn$ (not shown; *Henderson* et al., 1989), all white micas plot in the zinnwaldite field.

Topaz from the Hongshan granites has high F contents, ranging from 16.5 to 18.3 wt.% (Table 1), similar to those from other topaz-bearing granites (*Manning* and *Hill*, 1990; *Taylor*, 1992) and close to the theoretical maximum of 20.7 wt.% (*Deer* et al., 1966), suggesting a primary magmatic origin (*Foord* et al., 1992; *Liu* et al., 1999; *Kesraoui* and *Nedjari*, 2002). Tourmalines in the Hongshan granites are schorl with very high Fe/(Mg + Fe) ratios (0.84–0.89) and Na/(Na + Ca) ratios (0.94–0.99). They plot in the field of tourmalines from Li-rich granitic pegmatites and aplites in the Al–Fe–Mg ternary diagram (*Henry* and *Guidotti*, 1985); they are distinct from those of metamorphic origin, and consistent with a magmatic origin.

Table 1. *Mineral compositions of the Hongshan granites*

Sample no.	TX-117-2						TX-123-1				TX-127		
Minerals	Ab	Kf	Bt	Ms	Toz	Tur	Ab	Bt	Ms	Toz	Ab-r	Ab-c	Kf
Avg no.	1	2	3	2	3	1	2	1	3	2	1	3	2
SiO_2	67.73	63.83	39.15	46.80	32.91	33.26	68.58	38.41	47.74	33.43	68.61	68.39	63.92
TiO_2	0.02	0.02	0.92	0.29	n.a.	0.37	0.00	0.76	0.33	n.a.	0.01	0.01	0.00
Al_2O_3	19.87	19.28	24.18	32.90	56.13	33.04	19.40	22.84	30.57	58.09	19.57	19.12	19.24
FeO	0.10	0.15	19.01	4.33	0.01	15.47	0.03	21.51	5.28	0.04	0.05	0.00	0.05
MnO	b.d.	0.05	1.20	0.23	0.01	0.48	0.00	0.94	0.22	0.03	b.d.	0.00	0.03
MgO	0.01	0.00	1.51	0.78	0.00	1.07	0.01	1.62	1.24	0.00	b.d.	0.01	0.00
CaO	0.22	0.07	0.01	0.01	0.01	0.04	0.11	b.d.	0.05	0.03	b.d.	0.47	0.01
Na_2O	11.17	0.14	0.23	0.33	n.a.	1.76	11.77	0.13	0.17	n.a.	11.77	11.26	0.25
K_2O	0.21	15.77	8.85	9.99	0.01	0.05	0.10	8.85	10.01	0.02	0.10	0.14	16.12
F					17.21	0.15				16.96			
Total	99.33	99.31	95.07	95.67	99.04	85.62	99.99	95.04	95.60	101.46	100.11	99.39	99.63
$Mg^{\#}$			0.12	0.24		0.11		0.12	0.29				
An%	1.08	0.38					0.50				0.00	2.21	0.06
Ab%	97.7	1.31					99.0				99.5	96.98	2.30
Or%	1.21	98.31					0.55				0.53	0.81	97.60

Sample no.	TX-127			TX-125-1				TX-125-2					
Minerals	Bt	Ms	Toz	Ab	Kf	Ms	Toz	Ab	Kf	Bt	Ms	Toz	Tur
Avg no.	1	4	4	3	3	4	3	3	2	4	4	2	2
SiO_2	36.01	46.19	32.59	68.38	63.69	46.63	33.43	68.67	64.01	38.87	45.58	33.26	34.81
TiO_2	1.81	0.26	n.a.	0.00	0.00	0.21	n.a.	0.00	0.00	0.90	0.27	n.a.	0.51
Al_2O_3	23.01	31.44	55.01	19.50	19.57	32.89	57.58	19.72	19.33	23.74	28.23	57.11	34.61
FeO	23.18	5.99	0.02	0.00	0.05	5.50	0.01	0.07	0.05	19.48	9.35	0.06	16.30
MnO	1.23	0.37	0.03	0.01	0.02	0.27	0.02	0.02	0.05	1.39	0.60	0.01	0.40
MgO	1.65	0.92	0.00	0.02	0.00	0.64	0.00	0.00	0.00	1.46	0.99	0.00	1.10
CaO	0.02	0.01	0.01	0.37	0.01	0.05	0.02	0.15	0.02	0.01	0.01	0.01	0.03
Na_2O	0.14	0.26	n.a.	11.16	0.25	0.34	n.a.	11.18	0.31	0.26	0.22	n.a.	2.24
K_2O	8.94	9.88	0.00	0.18	15.77	9.57	0.01	0.11	15.89	9.08	10.22	0.01	0.03
F			16.87				17.01					18.30	0.11
Total	96.00	95.33	97.43	99.62	99.37	96.10	100.92	99.92	99.66	95.20	95.47	101.04	90.09
$Mg^{\#}$	0.11	0.22	0.12			0.17				0.12	0.16		0.11
An%				1.76	0.03			0.74	0.09				
Ab%				97.2	2.4			98.6	2.9				
Or%				1.02	97.60			0.61	97.01				

Sample no.	TX-126-1				TX-132					TX-133-1			
Minerals	Ab	Kf	Bt	Ms	Ab	Kf	Ms	Toz	Tur	Ab	Kf	Bt	Ms
Avg no.	3	3	1	4	3	6	4	3	2	1	3	2	1
SiO_2	68.16	64.08	38.95	45.52	68.27	63.88	47.18	32.77	33.48	66.94	63.90	34.86	47.10
TiO_2	0.02	0.00	0.95	0.41	0.00	0.00	0.30	n.a.	0.85	b.d.	0.04	2.23	0.03
Al_2O_3	20.01	19.26	25.18	28.03	20.06	19.26	30.58	56.24	32.95	20.37	19.69	20.39	34.63

(*continued*)

Table 1 (*continued*)

Sample no.	TX-126-1				TX-132					TX-133-1			
Minerals	Ab	Kf	Bt	Ms	Ab	Kf	Ms	Toz	Tur	Ab	Kf	Bt	Ms
Avg no.	3	3	1	4	3	6	4	3	2	1	3	2	1
FeO	0.02	0.08	17.19	10.01	0.06	0.01	5.23	0.03	15.67	0.18	0.04	25.73	2.37
MnO	0.03	0.02	1.18	0.78	0.02	0.13	0.13	0.01	0.21	b.d.	0.03	0.95	0.13
MgO	0.04	0.00	1.52	1.20	0.02	0.00	1.52	0.00	1.70	0.04	0.00	2.83	0.42
CaO	0.24	0.18	b.d.	0.01	0.18	0.03	0.01	0.01	0.25	0.13	0.05	0.01	0.02
Na_2O	11.13	0.24	0.24	0.26	11.12	0.34	0.26	n.a.	2.23	10.15	1.02	0.06	0.39
K_2O	0.10	15.79	9.74	9.92	0.08	15.80	10.35	0.01	0.06	1.35	14.72	9.11	10.44
F								16.52	1.31				
Total	99.74	99.65	94.95	96.14	99.81	99.45	95.57	98.64	88.18	99.15	99.48	96.16	95.54
$Mg^{\#}$			0.14	0.18			0.34		0.16			0.16	0.24
An%	1.15	0.91			0.88	0.13				0.62	0.27		
Ab%	98.3	2.2			98.7	3.2				91.4	9.5		
Or%	0.58	96.87			0.45	96.71				7.98	90.25		

Ab Albite, *Kf* K-feldspar, *Bt* biotite, *Ms* muscovite, *Toz* topaz, *Tur* tourmaline; *n.a.* not analysed, *b.d.* below detection limit; $Mg^{\#} = Mg/(Mg + Fe)$ atom%

Whole-rock geochemistry

Major elements

The Hongshan granites have a limited compositional range in bulk-rock major-element chemistry, and are characterized by high SiO_2 (>74 wt.%) and K_2O (4.37–5.05 wt.%), and low CaO (0.33–0.79 wt.%), MgO (<0.27 wt.%) and P_2O_5 (0.07–0.17 wt.%) (Table 2). Their aluminum saturation index (ASI) and F contents range from 1.11 to 1.35 and 0.23 to 0.56 wt.%, respectively, indicating that they are strongly peraluminous, F-rich granites. F-rich topaz-bearing granite can be classified into high-P and low-P subtypes (*Taylor*, 1992; *London*, 1992). The high-P subtype has $P_2O_5 > 0.4$ wt.%, $Al_2O_3 > 14.5$ wt.%, $SiO_2 < 73$ wt.%, and the low-P subtype has $P_2O_5 < 0.1$ wt.%, $Al_2O_3 < 14.5$ wt.%, $SiO_2 > 73$ wt.%. Thus the Hongshan topaz-bearing granites belong to the low-P subtype based on their low P_2O_5 (0.12 wt.% average) and Al_2O_3 (12.85 wt.%), and high SiO_2 (75.38 wt.%). Compared to other low-P topaz-bearing granites, such as those from Pleasant Ridge, Canada (*Taylor*, 1992), Yanbei, China (*Liu* et al., 1999) and Pintinga, Brazil (*Lenharo* et al., 2003), the Hongshan granites have relatively high MgO (>0.11 wt.%), TiO_2 (>0.12 wt.%), and K_2O/Na_2O (1.29–1.85), and lower F contents (Table 2).

The SiO_2 content of the Hongshan granites shows little variation (74–77 wt.%) and does not correlate well with most elements, including trace elements, except for rough negative correlations with Al_2O_3 and $K_2O + Na_2O$ (Fig. 3a, b), which may reflect small variations in the modal abundance of quartz and feldspar. However, some element ratios and F contents correlate well with total mafic components ($TFMM = TiO_2 + FeO + Fe_2O_3 + MgO + MnO$; Fig. 3c–e). K_2O/Na_2O and CaO/Na_2O correlate positively with TFMM, whereas Al_2O_3/TiO_2, ASI index and F contents correlate negatively. In general, the mafic components (TFMM) decrease

Table 2. *Major- and trace-element compositions of the Hongshan granites and wall-rocks*

Sample no.	TX-121	TX-132	TX-133-1	TX-130	TX-131	TX-128	TX-115	TX-120	TX-123-2	TX-126-1	TX-123-1	TX-116-2	TX-127	TX-117-2	TX-125-1	Wall-rock
SiO_2	74.17	74.90	75.11	76.07	76.14	77.03	74.20	77.05	74.64	74.08	75.23	76.34	76.48	74.50	74.73	70.72
TiO_2	0.24	0.21	0.22	0.18	0.16	0.22	0.17	0.18	0.16	0.15	0.14	0.18	0.15	0.13	0.12	0.64
Al_2O_3	13.20	12.38	12.37	12.19	12.72	11.77	13.41	11.86	13.18	13.59	13.01	12.45	12.63	13.73	14.19	12.49
Fe_2O_3	0.66	0.70	0.69	0.63	0.24	0.63	0.36	0.44	0.50	0.34	0.37	0.33	0.40	0.42	0.29	2.26
FeO	1.42	1.23	1.26	1.14	1.33	1.24	1.35	1.27	1.17	1.19	1.18	1.10	1.03	1.03	0.92	2.64
MnO	0.05	0.05	0.05	0.05	0.04	0.05	0.07	0.05	0.06	0.09	0.06	0.05	0.05	0.06	0.07	0.08
MgO	0.27	0.24	0.19	0.19	0.12	0.22	0.17	0.15	0.14	0.12	0.13	0.14	0.15	0.11	0.16	2.06
CaO	0.56	0.79	0.72	0.57	0.46	0.53	0.50	0.46	0.63	0.51	0.51	0.54	0.41	0.61	0.33	1.55
Na_2O	2.91	2.86	2.99	2.89	2.66	2.62	3.42	2.77	3.36	3.51	3.10	3.02	3.20	3.39	2.81	1.44
K_2O	5.05	4.74	4.53	4.37	4.91	4.51	4.83	4.45	4.80	4.52	4.88	4.46	4.45	4.63	4.90	3.02
P_2O_5	0.17	0.12	0.10	0.08	0.07	0.10	0.12	0.12	0.12	0.14	0.12	0.14	0.13	0.15	0.12	0.13
F	–	0.33	0.30	0.31	0.29	0.23	0.25	–	–	0.40	0.38	–	0.36	0.52	0.56	–
LOI	1.12	1.4	1.44	1.46	1.07	0.85	1.15	1.02	1.07	1.24	1.01	0.99	0.94	1.14	1.30	2.65
Total	99.82	99.81	99.84	100.0	100.1	99.9	99.90	99.82	99.83	99.71	99.96	99.74	100.2	100.2	100.3	99.78
ASI	1.17	1.10	1.11	1.16	1.21	1.16	1.14	1.16	1.11	1.17	1.15	1.16	1.17	1.17	1.35	1.47
K_2O/Na_2O	1.74	1.66	1.52	1.51	1.85	1.72	1.41	1.61	1.43	1.29	1.57	1.48	1.39	1.37	1.74	2.10
CaO/Na_2O	0.192	0.276	0.241	0.197	0.173	0.202	0.146	0.166	0.188	0.145	0.165	0.179	0.128	0.180	0.117	1.08
Al_2O_3/TiO_2	55.0	59.0	56.2	67.7	79.5	53.5	78.9	65.9	82.4	90.6	92.9	69.2	84.2	105.6	118.3	19.6
Rb	388	327	375	456	383	439	440	437	539	626	527	487	535	583	747	139
Cs	21.9	12.9	13.5	16.9	15.2	13.7	13.6	17.7	26.9	39.9	25.9	21.5	28.3	44.0	33.9	5.90
Sr	41.5	31.5	33.9	16.7	27.1	14.6	25.9	16.9	18.7	14.5	18.4	20.2	12.9	19.4	10.6	95.3
Ba	136	115	99.9	45.5	104	27.4	70.8	41.9	60.4	40.5	55.8	66.4	39.8	41.2	25.1	658
Zr	133	110	126	106	119	82.1	80.5	90.2	72.5	58.2	64.0	78.2	63.5	46.1	26.9	275
Hf	5.13	4.50	4.99	4.55	4.95	3.69	3.43	4.03	3.19	2.97	2.85	3.53	3.17	2.40	1.51	8.03
Nb	24.3	22.5	27.0	27.4	27.6	22.8	28.3	25.5	26.1	33.8	25.1	32.8	31.1	30.3	36.7	17.7
Ta	3.54	3.56	4.21	4.02	3.37	3.54	5.00	4.01	4.04	7.09	4.38	7.31	6.00	6.58	4.62	1.28
Y	43.5	48.5	56.3	50.2	52.4	34.1	36.6	32.5	37.6	27.5	32.2	31.4	24.9	20.9	15.7	32.9
Sn	17.6	15.3	18.2	20.8	19.7	16.0	26.2	20.8	24.6	38.8	29.4	25.4	30.8	30.7	54.0	3.02
Sb	0.53	0.74	0.78	1.06	0.36	1.05	0.76	1.38	0.50	1.06	0.88	0.76	0.63	0.59	0.49	1.23
W	7.9	7.2	6.4	5.5	6.5	3.0	4.3	7.2	7.9	8.5	7.1	11.6	10.7	11.9	14.9	3.38
Pb	32.5	29.7	32.5	29.0	31.2	32.6	26.3	28.2	34.3	19.6	27.5	20.8	21.8	21.6	16.3	14.61
Th	35.7	36.4	34.6	32.6	37.4	27.4	22.8	26.0	24.1	19.1	21.8	21.4	18.4	13.8	12.1	15.21
U	6.8	14.4	19.0	19.8	15.9	30.3	19.3	24.4	19.9	28.8	14.8	18.5	24.1	28.1	6.0	2.58
Sc	3.64	3.69	4.14	2.00	3.56	2.55	5.04	1.89	3.72	2.85	1.90	3.56	2.57	3.44	6.01	10.68

(*continued*)

Table 2 (*continued*)

Sample no.	TX-121	TX-132	TX-133-1	TX-130	TX-131	TX-128	TX-115	TX-120	TX-123-2	TX-126-1	TX-123-1	TX-116-2	TX-127	TX-117-2	TX-125-1	Wall-rock
V	12.81	8.73	8.81	7.02	7.26	7.55	5.96	5.13	6.23	4.11	4.86	5.61	3.44	6.64	3.34	77.76
Cr	8.85	8.39	13.56	4.96	5.92	3.70	9.73	3.84	4.57	7.41	8.40	10.63	14.27	13.61	4.19	75.06
Co	1.87	1.72	1.54	1.15	1.73	1.07	1.07	1.15	1.25	0.91	1.10	0.94	0.82	0.69	0.61	10.91
Ni	3.90	2.99	6.01	2.34	3.06	2.34	3.91	2.04	2.74	3.34	4.71	6.63	6.92	6.97	1.34	30.10
Zn	51.0	29.3	40.7	38.0	49.2	39.4	39.5	43.2	38.8	38.8	44.0	40.2	30.1	31.9	34.8	107.4
Ga	20.2	18.3	18.9	17.2	18.0	13.8	20.2	14.0	20.3	21.6	19.5	17.9	17.9	20.9	25.1	17.1
La	40.1	38.7	35.1	27.8	37.8	19.2	19.7	20.0	19.4	11.7	16.6	17.1	13.0	8.3	7.3	47.6
Ce	93.57	90.11	81.42	67.93	84.62	54.67	45.55	55.98	46.80	30.56	41.14	41.99	32.48	19.89	19.28	93.8
Pr	10.32	9.44	8.70	7.14	9.25	5.17	4.90	5.44	4.87	3.29	4.43	4.54	3.46	2.23	1.94	9.86
Nd	37.5	35.6	30.8	25.9	34.4	19.4	18.2	20.1	18.0	12.3	16.8	16.6	13.3	8.3	7.1	36.0
Sm	8.58	8.32	7.48	6.35	7.97	4.65	4.88	5.06	4.57	3.55	4.28	4.24	3.76	2.63	2.04	6.96
Eu	0.40	0.33	0.26	0.16	0.27	0.10	0.17	0.12	0.18	0.08	0.11	0.13	0.07	0.07	0.04	1.21
Gd	7.44	6.83	6.73	6.02	7.01	4.00	4.26	4.18	4.22	3.42	3.91	3.87	2.92	2.48	1.82	6.07
Tb	1.36	1.33	1.39	1.26	1.40	0.87	0.95	0.86	0.95	0.74	0.83	0.80	0.69	0.54	0.41	0.96
Dy	8.15	8.45	9.37	8.78	8.83	5.93	6.15	5.57	6.34	4.97	5.61	5.18	4.46	3.69	2.88	5.77
Ho	1.61	1.77	1.86	1.80	1.90	1.21	1.24	1.18	1.27	0.97	1.14	1.08	0.85	0.76	0.54	1.19
Er	4.74	5.14	6.04	5.56	5.74	3.81	3.81	3.73	4.13	2.99	3.51	3.18	2.60	2.20	1.67	3.42
Tm	0.67	0.80	0.91	0.86	0.85	0.58	0.62	0.56	0.62	0.55	0.56	0.52	0.43	0.37	0.27	0.51
Yb	4.56	5.41	6.30	5.90	6.06	4.43	4.37	3.99	4.54	3.69	3.91	3.99	3.08	2.92	2.08	3.44
Lu	0.64	0.80	0.96	0.87	0.91	0.60	0.64	0.56	0.66	0.55	0.54	0.55	0.47	0.42	0.32	0.52
REE	220	213	197	166	207	125	115	127	117	79	103	104	81.7	54.8	47.7	217
Eu/Eu*	0.15	0.13	0.11	0.08	0.11	0.07	0.11	0.08	0.12	0.07	0.08	0.10	0.06	0.08	0.07	0.55
(La/Yb)n	5.94	4.82	3.76	3.18	4.21	2.93	3.03	3.38	2.88	2.15	2.86	2.88	2.86	1.93	2.38	9.33
K/Rb	108	120	100	80	106	85	91	84	74	60	77	76	69	66	54	181
Rb/Sr	9.4	10.4	11.1	27.3	14.1	30.1	17.0	25.8	28.8	43.2	28.7	24.2	41.6	30.0	70.5	1.5
Nb/Ta	6.9	6.3	6.4	6.8	8.2	6.4	5.7	6.4	6.5	4.8	5.7	4.5	5.2	4.6	8.0	13.8
Zr/Hf	26.0	24.5	25.2	23.3	24.1	22.3	23.4	22.4	22.7	19.6	22.5	22.1	20.0	19.2	17.8	34.2
Y/Ho	27.0	27.5	30.2	28.0	27.5	28.2	29.5	27.5	29.6	28.2	28.2	29.0	29.3	27.5	29.0	27.7
Th/U	5.29	2.53	1.82	1.65	2.36	0.90	1.18	1.06	1.21	0.66	1.48	1.16	0.76	0.49	2.02	5.90
$TE_{1,3}$	1.08	1.07	1.12	1.12	1.06	1.17	1.13	1.14	1.14	1.15	1.12	1.12	1.16	1.13	1.19	
t (°C)	790	769	782	772	785	752	745	760	735	722	729	746	730	704	676	

Wall-rock composition is an average of nine Taoxi Group metamorphic rocks; ASI $= Al_2O_3/(CaO + Na_2O + K_2O)$ mol; Eu/Eu* $= 2\times(Eu)n/(Sm + Gd)n$; $TE_{1,3}$ was calculated according to *Irber* (1999)'s quantified equation; Temperature was calculated according to *Watson* and *Harrison* (1983)'s thermometer

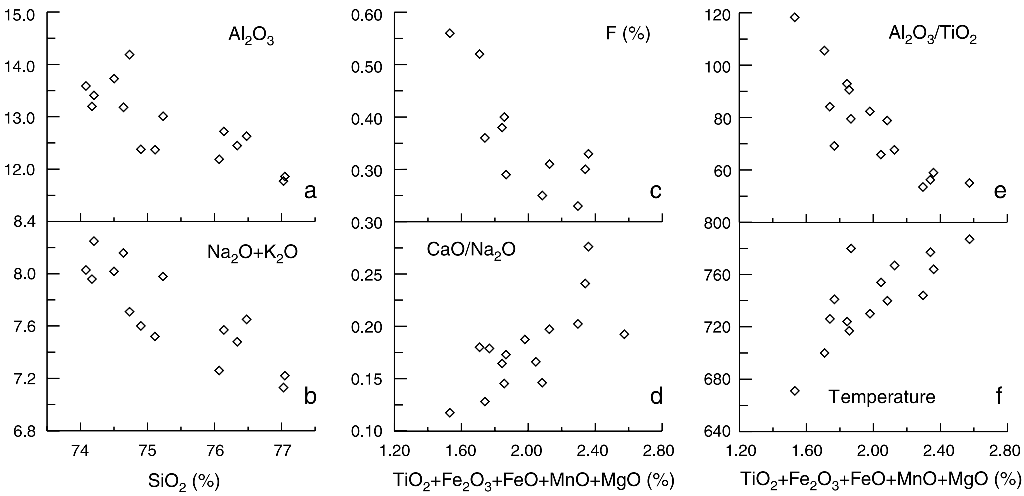

Fig. 3. Correlations of SiO_2 and $TiO_2 + Fe_2O_3 + FeO + MnO + MgO$ wt.% (TFMM) with some major elements, element ratios and temperature of the Hongshan granites. Temperatures are based on the zircon saturation thermometer (Table 2; *Watson* and *Harrison*, 1983)

with progressive magma evolution, consequently F contents, ASI index and modal albite increases with evolution, which is consistent with concomitant decreasing crystallization temperatures (Fig. 3f).

Trace elements

The Hongshan granites have relatively high contents of Rb, Cs, Nb, Ta, Sn, Th and U, and very low contents of Ba, Sr, Zr, Hf, Eu and transition metals (Table 2, Fig. 4a),

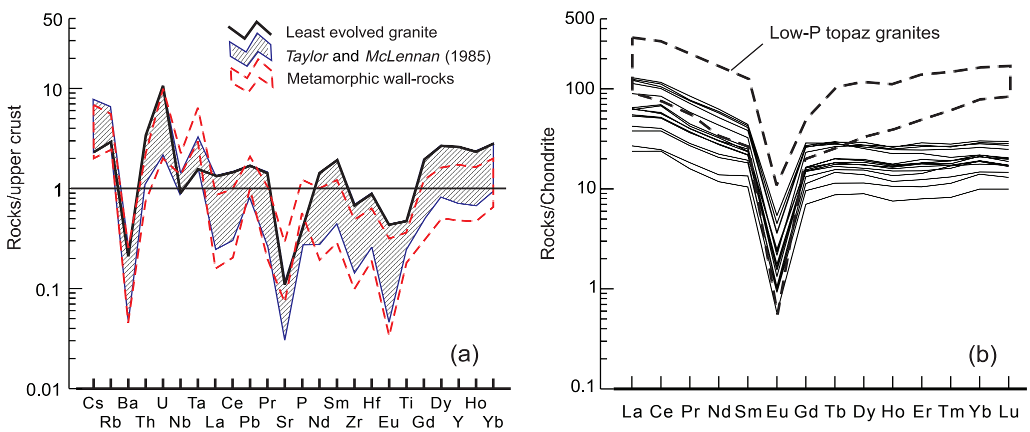

Fig. 4. Normalized trace-element abundance distribution of the Hongshan granites. (**a**) Incompatible element patterns of the Hongshan granites normalized to the upper crust composition and metamorphic wall rocks. The metamorphic wall rocks are from the Neoproterozoic Taoxi Group and Louziba Formation (Table 2); the least evolved Hongshan granite is determined based on composition variation trend. Normalization factors from *Taylor* and *McLennan* (1985). (**b**) Chondrite-normalized REE patterns. Low-P topaz granites are from *Taylor* (1992) and *Lenharo* et al. (2003). Normalization factors from *Boynton* (1984)

typical of many topaz-bearing granites. In particular, they exhibit very low K/Rb, Nb/Ta, Zr/Hf and Th/U and extremely high Rb/Sr, and thus are markedly different from typical I- and S-type granites (*Whalen* et al., 1987). However, compared with typical low-P topaz-bearing granites (*Taylor*, 1992; *Liu* et al., 1999; *Lenharo* et al., 2003), the Hongshan granites show lower concentrations of Rb, Cs, Ba, Nb, Ta, Hf, Y, W, Pb, REE, lower Rb/Sr, and higher K/Rb, Nb/Ta, Zr/Hf and La/Yb.

The Hongshan granites have rare-earth element (REE) patterns with weak REE fractionation and strong negative Eu anomalies (Fig. 4b). Their REE totals are lower than those of many typical topaz granites (Fig. 4b; *Taylor*, 1992; *Lenharo* et al., 2003); (La/Yb)n ratios change from 5.94 to 1.93 (average of 3.28) and Eu/Eu* from 0.15 to 0.06 (average 0.09).

Although the major elements of the Hongshan granites show limited variation, their trace elements show large variations and good correlations with TFMM, F contents and CaO/Na_2O (Fig. 5). There is a factor of 4–5 difference in some trace-element contents, such as Zr, Ba and REE, between the strongly and weakly evolved samples. As TFMM decreases, Rb, Cs, Nb, Ta, Sn and W increase while Sr, Ba, Zr, Hf, Y, REE, Pb, Th and transition metals decrease. In addition, (La/Yb)n, K/Rb, Zr/Hf, Th/U and Eu/Eu* all decrease significantly, whereas Rb/Sr increases. These variations probably reflect changes in accessory-mineral abundance; in particular variations in Zr, Hf, Nb, Ta, Th, U and HREE may be mainly controlled by zircon, monazite and ilmenite.

Highly fractionated rocks are saturated in zircon; therefore Zr contents can be used to estimate the crystallization temperature using zircon saturation thermometry (*Watson* and *Harrison*, 1983). These calculations indicate that the Hongshan granites formed at low temperatures (790–676 °C; Table 2); the calculated temperatures shows a positive correlation with TFMM (Fig. 3f). Therefore, the variations

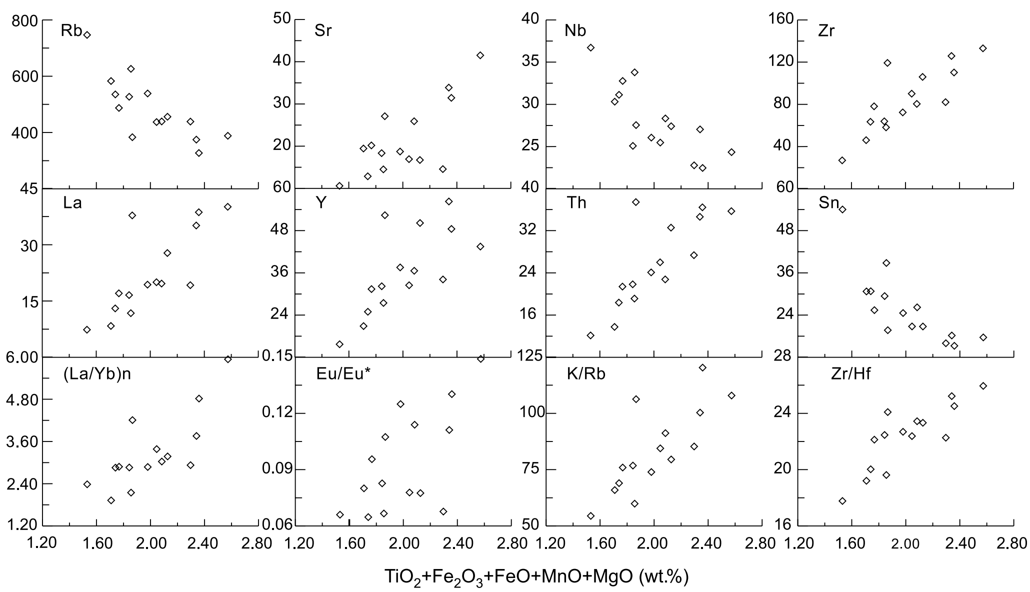

Fig. 5. Correlations of TiO_2–Fe_2O_3–FeO–MnO–MgO (TFMM) with some incompatible trace elements and element ratios of the Hongshan granites

in geochemical parameters with TFMM reflect changes in crystallization temperature of the magma, corresponding well with the magmatic fractionation model.

U–Pb dating of zircon

BSE/CL images of zircons

Three Hongshan granite samples were chosen for zircon separation. Zircons were obtained from two samples (TX-120, TX-121), but not from sample TX-127; this is probably due to the low zirconium content (Zr = 63 ppm) and the small volume (~2.5 kg) of the sample that was crushed. The zircon BSE/CL images reveal complex internal structures. Most zircon grains have good crystal forms with generally concentric, oscillatory zoning and no inherited core (Fig. 6a–c). Rare zircon grains contain small, irregular inherited cores (Fig. 6d). The inherited zircon cores are designated here as phase I (P-I). The concentrically zoned zircon grains and similar overgrowths on inherited cores are here designated as phase II (P-II) and comprise the main zircon population in these rocks. Another zircon type has low BSE/CL intensity with little obvious internal structure (Fig. 6e, f). These may occur as discrete euhedral or anhedral grains or may form outermost overgrowths on zoned zircon grains (Fig. 6c), and have been designated here as phase III (P-III). Some zircon grains show different internal structures, either euhedral prismatic with dark BSE/CL images and abundant cracks or irregular internal structure (e.g. grain TX-120-13, TX-120-26, Fig. 6h, i).

Some monazite grains were picked out from these three samples. Fine-grained euhedral monazites show homogeneous inner structure and very high BSE intensity, probably reflecting high contents of ThO_2 (7.64 wt.%) and UO_2 (0.86 wt.%). Large monazite fragments have light-grey domains with brighter irregular rims.

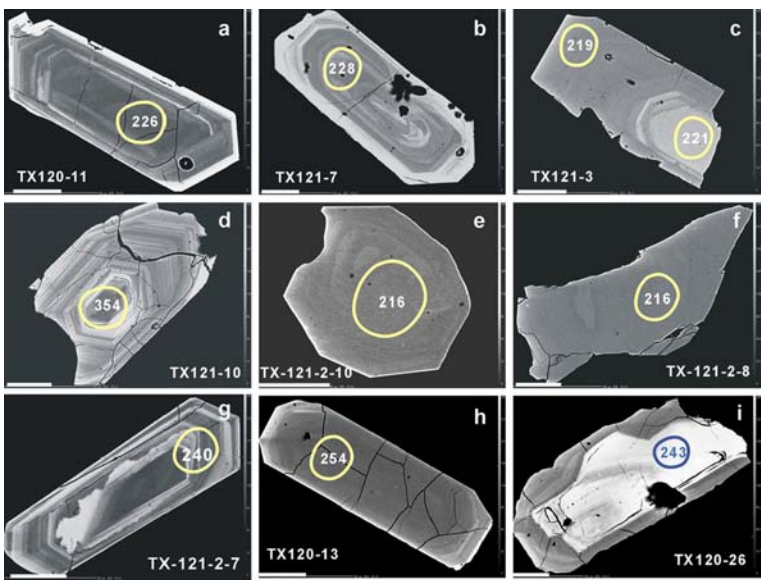

Fig. 6. BSE/CL images and U–Pb dating positions of zircons from the Hongshan granites. Numbers in circles are $^{206}Pb/^{238}U$ ages in Ma; scale bars are 50 μm

Table 3. *Laser ablation ICPMS U–Pb data and calculated ages for zircons and monazites from the Hongshan granites*

Grain#	Phase	Isotopic ratios						Ages (Ma)						Corrected common Pb (%)
		$\frac{^{206}Pb}{^{238}U}$	$\pm 1\sigma$	$\frac{^{207}Pb}{^{235}U}$	$\pm 1\sigma$	$\frac{^{207}Pb}{^{206}Pb}$	$\pm 1\sigma$	$\frac{^{206}Pb}{^{238}U}$	1σ	$\frac{^{207}Pb}{^{235}U}$	1σ	$\frac{^{207}Pb}{^{206}Pb}$	1σ	
TX-121														
−10c	I + II	0.05645	0.00074	0.46190	0.01427	0.05934	0.00199	354	5	386	10	580	75	4.93
−11r		0.03950	0.00051	0.28505	0.00371	0.05234	0.00055	250	3	255	3	300	25	
−2–7		0.03800	0.00043	0.26735	0.00319	0.05103	0.00055	240	3	241	3	242	25	
−2–3		0.03785	0.00044	0.26345	0.00326	0.05048	0.00057	239	3	237	3	217	27	
−2–16		0.03758	0.00043	0.26141	0.00325	0.05045	0.00058	238	3	236	3	216	27	
−12c	II	0.03703	0.00047	0.26734	0.00387	0.05238	0.00067	234	3	241	3	302	30	0.32
−2r	II	0.03655	0.00046	0.25933	0.00347	0.05153	0.00059	231	3	234	3	265	27	
−2–8	III	0.03626	0.00073	0.35212	0.01613	0.07045	0.00337	230	5	306	12	941	101	−1.2
−7c	II	0.03602	0.00051	0.27290	0.00916	0.05495	0.00200	228	3	245	7	410	83	1.15
−2–12	Mona	0.03594	0.00043	0.36129	0.00456	0.07293	0.00081	228	3	313	3	1012	23	
−2–2	II	0.03591	0.00046	0.24689	0.00806	0.04987	0.00175	227	3	224	7	189	83	0.35
−2–6	II	0.03591	0.00044	0.25716	0.00501	0.05193	0.00100	227	3	232	4	282	45	
−2c	II	0.03560	0.00045	0.28403	0.00407	0.05788	0.00074	226	3	254	3	525	29	−0.61
−8	III	0.03571	0.00053	0.25222	0.00802	0.05125	0.00164	226	3	228	7	252	75	
−2–11	II	0.03575	0.00041	0.24834	0.00322	0.05041	0.00061	226	3	225	3	214	29	
−6–17r	II	0.03572	0.00045	0.28830	0.00384	0.05856	0.00067	226	3	257	3	551	26	
−4c	II	0.03518	0.00047	0.25234	0.00522	0.05202	0.00103	223	3	228	4	286	46	
−6c	II	0.03515	0.00055	0.31405	0.01767	0.06480	0.00379	223	3	277	14	768	126	6.86
−3c	II	0.03483	0.00045	0.25391	0.00400	0.05291	0.00076	221	3	230	3	325	33	−0.31
−5r	III	0.03493	0.00053	0.30805	0.01533	0.06396	0.00333	221	3	273	12	740	113	5.31
−3r	III	0.03456	0.00047	0.25784	0.00643	0.05414	0.00132	219	3	233	5	377	56	−0.1
−15	III	0.03459	0.00048	0.26795	0.00694	0.05621	0.00144	219	3	241	6	461	58	0.28
−2–13	II	0.03437	0.00041	0.24103	0.00575	0.05086	0.00136	218	3	219	5	235	63	0.4

(continued)

Table 3 (*continued*)

Grain#	Phase	Isotopic ratios						Ages (Ma)						Corrected common Pb (%)
		$^{206}Pb/^{238}U$	±1σ	$^{207}Pb/^{235}U$	±1σ	$^{207}Pb/^{206}Pb$	±1σ	$^{206}Pb/^{238}U$	1σ	$^{207}Pb/^{235}U$	1σ	$^{207}Pb/^{206}Pb$	1σ	
−2–14	II	0.03433	0.00040	0.25657	0.00397	0.05424	0.00082	218	2	232	3	381	35	0.24
−2–10	III	0.03411	0.00041	0.24847	0.00431	0.05285	0.00090	216	3	225	4	322	40	0.3
−6–20	III	0.03413	0.00044	0.24904	0.00408	0.05293	0.00081	216	3	226	3	326	36	
−13r	III	0.03391	0.00044	0.33763	0.00569	0.07225	0.00115	215	3	295	4	993	33	
−2–9	III	0.03394	0.00040	0.24041	0.00373	0.05140	0.00077	215	2	219	3	259	35	
−1c	III	0.03374	0.00056	0.28057	0.01666	0.06031	0.00372	214	3	251	13	615	137	2.56
TX-120														
−13		0.04024	0.00047	0.29762	0.00746	0.05364	0.00148	254	3	265	6	356	64	3.08
−22		0.03843	0.00043	0.27850	0.00463	0.05257	0.00105	243	3	249	4	310	47	0.19
−26		0.03834	0.00046	0.26879	0.00338	0.05084	0.00057	243	3	242	3	234	26	
−24	II	0.03672	0.00045	0.26326	0.00495	0.05199	0.00096	232	3	237	4	285	43	
−3	II	0.03635	0.00044	0.25550	0.00369	0.05098	0.00069	230	3	231	3	240	32	
−11	II	0.03567	0.00045	0.24859	0.00890	0.05055	0.00192	226	3	225	7	220	90	1.18
−19	II	0.03532	0.00046	0.24513	0.00949	0.05033	0.00206	224	3	223	8	210	97	1.96
−14	II	0.03516	0.00047	0.24242	0.01052	0.05001	0.00227	223	3	220	9	195	106	2.01
−21	II	0.03507	0.00042	0.24301	0.00411	0.05024	0.00083	222	3	221	3	206	39	
TX-127														
−2	Mona	0.04470	0.00056	0.32664	0.00404	0.05300	0.00053	282	3	287	3	329	23	
−4	Mona	0.04427	0.00055	0.47538	0.00591	0.07785	0.00080	279	3	395	4	1143	21	

Mona Monazite

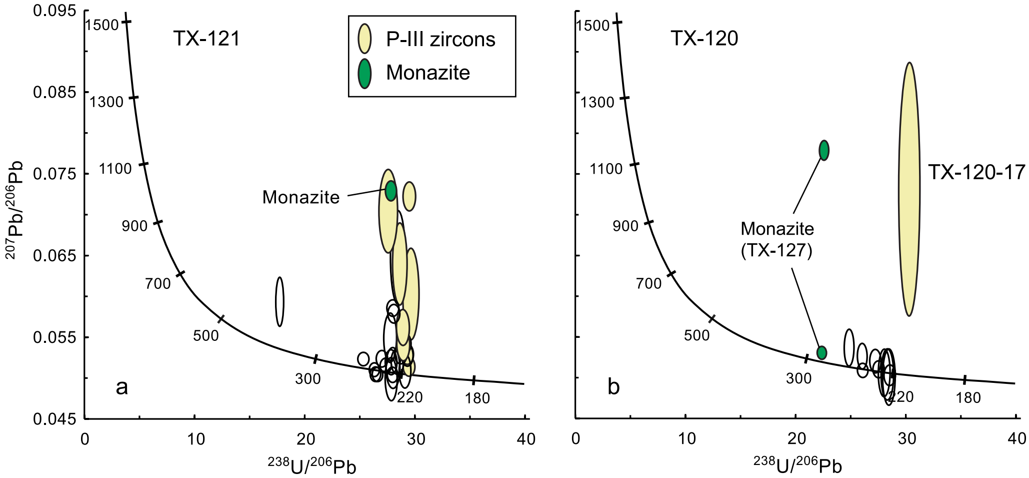

Fig. 7. U–Pb concordia diagrams of zircons from the Hongshan granites (calculated using Isoplot/Ex version 2.49, *Ludwig*, 2001)

Light-grey domains have the lowest ThO_2 (2.52 wt.%) and UO_2 (0.37 wt.%), and brighter parts have slightly higher ThO_2 (4.77 wt.%) and UO_2 (0.52 wt.%). These features suggest that the two types of monazites have different origins.

U–Pb dating results

Thirty-five separated zircon grains from samples TX-120 and TX-121, and three monazite grains from TX-121 and TX-127 were selected for U–Pb dating by LAM-ICPMS. Analytical results were corrected for common Pb based on the method of *Andersen* (2002), and only six grains need more than 2% common Pb correction (Table 3). The corrected $^{206}Pb/^{238}U$ ages are used in the following discussion.

The zircon U–Pb dating results for both rocks show a small age range for major P-II zircons (218–232 Ma, Table 3, Fig. 7). Only one P-I-type inherited core was large enough to be analyzed, and it gives an age of 354 Ma, about 100 Ma older than any of the P-II or P-III zircon grains. However, this analysis of the P-I core probably contains a component of the P-II zircon type because of its small size (Fig. 6d), hence 354 Ma can be interpreted as representing a minimum age.

The P-II zircon grains with concordance of >80% in sample TX-121 give ages from 218 ± 2 to 231 ± 3 Ma and those in sample TX-120 range from 222 ± 3 to 232 ± 3 Ma (Fig. 7), indicating that the Hongshan granites crystallized in early Mesozoic time. The P-III zircon grains give generally younger ages, but are mostly discordant (Table 3, Fig. 7), which may reflect late hydrothermal alteration effects. Those grains with unusual internal structures yielded older ages, 254–238 Ma (Fig. 6g–i). They do not show P-II overgrowths and have different Hf isotopic compositions from P-II zircons (see below), implying that they probably are xenocrysts.

One fine-grained monazite with high Th and U contents yields a similar age (228 Ma) to most P-II zircons, suggesting that it also crystallized from the same highly evolved magma as the zircons. However, two larger monazite fragments with different compositions give significantly older U–Pb ages (279 and 282 Ma, Table 3), suggesting that they formed possibly in an earlier thermal event in the area.

Table 4. *Rb–Sr and Sm–Nd isotopic compositions of the Hongshan granites*

Sample no.	TX-121	TX-133-1	TX-130	TX-131	TX-115	TX-126-1	TX-116-2	TX-127	TX-117-2	TX-125-1
Rb (ppm)	486.3	484	498.6	454.2	486.4	714.7	559.3	596.2	673.6	861
Sr (ppm)	38.03	33.63	15.63	27.37	25.39	13.5	19.98	13.33	19.94	11.42
$^{87}Rb/^{86}Sr$	37.40	42.14	94.56	48.74	56.42	159.56	82.94	134.0	100.6	232.0
$^{87}Sr/^{86}Sr$	0.819134	0.829804	0.959265	0.861085	0.890532	1.137292	0.956237	1.070021	1.000475	1.354966
2σ	0.000010	0.000012	0.000023	0.000010	0.000013	0.000038	0.000020	0.000014	0.000012	0.000014
I_{Sr} (225 Ma)	0.6994	0.6950	0.6567	0.7051	0.7100	0.6267	0.6908	0.6412	0.6785	0.6125
Sm (ppm)	7.858		6.194		4.722				2.600	2.350
Nd (ppm)	36.539		25.929		18.864				9.145	8.471
$^{147}Sm/^{144}Nd$	0.1301		0.1445		0.1514				0.1720	0.1678
$^{143}Nd/^{144}Nd$	0.512136		0.512112		0.512113				0.512108	0.511997
2σ	0.000008		0.000011		0.000009				0.000008	0.000011
I_{Nd} (225 Ma)	0.511944		0.511899		0.511890				0.511855	0.511750
εNd(t)	−7.88		−8.77		−8.94				−9.63	−11.68
T_{DM} (Ga)	1.64		1.72		1.73				1.79	1.95

T_{DM} Calculated based on two-stage model, assuming $^{147}Sm/^{144}Nd$ (crust) = 0.118

Sr–Nd–Hf isotopic compositions

Whole-rock Rb–Sr and Sm–Nd isotopes

Rb–Sr isotope analyses of ten whole-rock samples show that the Hongshan granites have high $^{87}Rb/^{86}Sr$ and $^{87}Sr/^{86}Sr$ ratios, 37.4–232 and 0.819–1.35, respectively (Table 4). An age of ca.187 ± 11 Ma may be calculated from the $^{87}Rb/^{86}Sr$ and $^{87}Sr/^{86}Sr$ regression line. However, as indicated by high MSWD value of 36, the regression line is not an isochron and the age is significantly different from the zircon U–Pb age (225 Ma, see below), hence it is not meaningful. On the other hand, unreasonably low initial $^{87}Sr/^{86}Sr$ ratios (0.613–0.699, Table 4) will be yielded, if the $^{87}Sr/^{86}Sr$ ratio of each sample is age-corrected to 225 Ma. These observations suggest that Rb and Sr were likely decoupled, that is the Rb–Sr isotopic system has not been closed following the granite crystallization.

The Hongshan granites have low εNd(t = 225 Ma) values, ranging from −7.9 to −11.7 (Table 4), similar to many strongly peraluminous granites in the Nanling belt (*Shen* et al., 1999; *Ling* et al., 2005; *Sun* et al., 2005). Such large variation in isotopic compositions may be due to heterogeneous source components, as proposed by *Deniel* et al. (1987) and *Krogstad* and *Walker* (1996). However, the $^{143}Nd/^{144}Nd$ of five samples also exhibits a weak negative correlation with $^{147}Sm/^{144}Nd$ and a positive correlation with TFMM abundances (Fig. 8), which cannot be explained by fractional crystallization alone. These correlations are most likely to result from assimilation of wall rocks with a low-$^{143}Nd/^{144}Nd$ component during the magma crystallization.

Lu–Hf isotopes of zircons

Lu–Hf isotopic analyses were carried out on seventeen zircon grains on which U–Pb dating had also been done. The $^{176}Hf/^{177}Hf$ ratios vary from 0.282274 to 0.282554 and their εHf(t = 225 Ma) from −12.3 to −2.9 (Table 5; Fig. 9). The

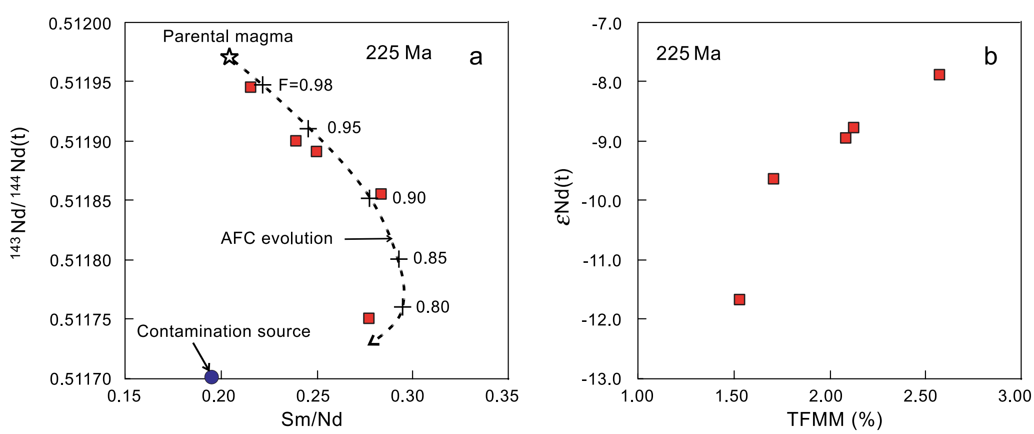

Fig. 8. $^{143}Nd/^{144}Nd$ vs Sm/Nd and TFMM diagrams of the Hongshan granites. In plot (**a**) F is the proportion of remaining melt in AFC modeling; all $^{143}Nd/^{144}Nd(t)$ values were calculated to 225 Ma. Detailed explanations are given in the text

Table 5. *Lu–Hf isotope ratios of zircons from the Hongshan granites*

Grain#		^{176}Hf/^{177}Hf	1σ	^{176}Lu/^{177}Hf	1σ	^{176}Yb/^{177}Hf	1σ	$T_{(DM)}{}^{C}$ (Ga)	εHf(t)	Age (Ma)
TX-121										
−2–7	II	0.282284	0.000018	0.003066	0.000120	0.081354	0.003100	2.05	−12.3	240
−2r	II	0.282479	0.000021	0.001159	0.000008	0.033567	0.000430	1.61	−5.3	231
−2–8	III	0.282447	0.000017	0.000650	0.000038	0.019567	0.001200	1.67	−6.4	230
−2c	II	0.282439	0.000032	0.000700	0.000017	0.024041	0.000790	1.70	−6.8	226
−8	III	0.282424	0.000016	0.000552	0.000006	0.015441	0.000062	1.73	−7.3	226
−2–11	II	0.282472	0.000021	0.001747	0.000080	0.047527	0.002200	1.63	−5.7	226
−4	II	0.282467	0.000021	0.000939	0.000012	0.026525	0.000400	1.64	−5.9	223
−6c	II	0.282537	0.000025	0.001064	0.000039	0.033592	0.001100	1.48	−3.4	223
−2–14	II	0.282554	0.000024	0.000733	0.000004	0.019799	0.000190	1.44	−2.9	218
−2–9	III	0.282460	0.000019	0.000911	0.000054	0.026788	0.001400	1.66	−6.3	215
TX-120										
−13	II	0.282274	0.000040	0.001491	0.000013	0.044238	0.000330	2.05	−12.1	254
−26	II	0.282400	0.000034	0.003000	0.000043	0.096391	0.001400	1.79	−8.1	243
−24	II	0.282457	0.000015	0.000517	0.000010	0.013626	0.000330	1.65	−6.0	232
−3	II	0.282473	0.000020	0.000739	0.000007	0.022023	0.000190	1.62	−5.5	230
−14	II	0.282417	0.000020	0.000995	0.000045	0.029824	0.001200	1.75	−7.6	223
−21	II	0.282458	0.000019	0.000955	0.000045	0.025851	0.001200	1.66	−6.2	222
−17	III	0.282438	0.000019	0.000703	0.000014	0.018988	0.000460	1.71	−7.2	209

Ages used for εHf(t) and $T_{(DM)}{}^{C}$ calculations are from Table 3; $\lambda^{176}\mathrm{Lu} = 1.865 \times 10^{-11}$, $T_{(DM)}{}^{C}$ is calculated based on two-stage model assuming ^{176}Lu/^{177}Hf of crust = 0.015 (*Griffin* et al., 2002)

negative εHf(t) values of all zircons indicate that the host magma was dominated by contributions from an old crustal source. The older zircons (xenocrysts) generally have the lowest ^{176}Hf/^{177}Hf and give Paleoproterozoic model ages. Their ^{176}Hf/^{177}Hf ratios are close to those for zircons of the nearby basement metamorphic wall-rocks of the Taoxi Group, assuming that these have evolved along the average crustal evolution line (^{176}Lu/^{177}Hf = 0.015, *Griffin* et al., 2002) to the early Mesozoic (Fig. 9). The dominant younger zircon population has relatively homogeneous Hf isotope compositions and less negative εHf(t); they all plot above the evolution trend of the Taoxi Group wall-rocks (Fig. 9) and have Mesoproterozoic model ages (1.4–1.7 Ga).

Petrogenesis of the Hongshan granites

Crystallization age of the Hongshan granites

According to the age distribution of zircons (Fig. 7) and their Hf isotopic compositions (Fig. 9), the zircons of the Hongshan granites most likely crystallized between 218 and 231 Ma. Seven zircons with concordance >90% give a weighted average ^{238}U/^{206}Pb age of 224.6 ± 2.3 Ma (MSWD = 1.6). In fact, all zircons with <235 Ma age yield the same average age, 224.6 ± 3.1 Ma, but with a larger uncertainty (MSWD = 9.3). Therefore it is suggested that the Hongshan granites formed

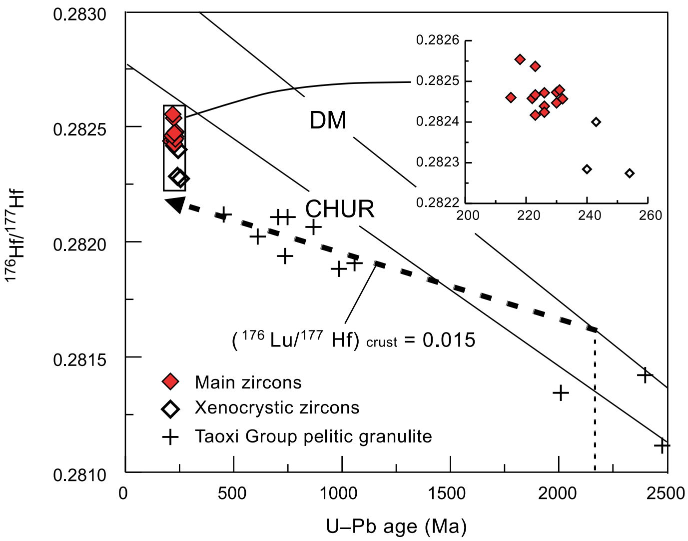

Fig. 9. $^{176}Hf/^{177}Hf$ vs age (Ma) for zircons from the two Hongshan granites and a Taoxi Group pelitic granulite. Grain TX-120-17 is not plotted due to its very large discordance and uncertainties (Fig. 7b, Table 3). Inset plot shows Hf-isotope difference between younger zircons and older (inherited) zircons. Hf-isotope data on zircons from the Taoxi granulite are from *Yu* et al. (2005), with metamorphic overgrowth zircons and anatectic zircons excluded. The Hf-isotope evolution of these detrital zircons suggests a Paleoproterozoic source

at ca. 225 Ma (lower Upper Triassic). Those zircons with unusual internal structures (Fig. 6g–i) give older ages, 240–254 Ma, and have lower Hf isotope ratios. They may have been incorporated as wall-rock fragments. The older monazites (~280 Ma) should have the same origin. These ages correspond to the late Paleozoic (Hercynian) magmatism and metamorphism occurring in the Cathaysia block (*Li* et al., 2006; *Yu* et al., 2006).

Source characteristics and generation of the Hongshan granitic magma

The high ASI index and K_2O/Na_2O, and low Nd and Hf isotopic ratios, suggest that the parental magma of the Hongshan granites was generated from old supracrustal rocks. U–Pb dating results for the zircon and monazite show that there have been several thermal events, including partial melting or metamorphism, from ~280 to 240 Ma in this area. Zircons with these older ages also have low Hf isotopic ratios and model ages of 1.8–2.1 Ga (Table 5). These isotopic features resemble those of nearby basement metamorphic rocks, such as the Zhoutan Group and Mayuan Group (*Xie* et al., 1996; *Hu* and *Zhang*, 1998), suggesting that they were the source rocks for the melt parental to these zircons.

The dominant younger zircons exhibit distinctly higher $^{176}Hf/^{177}Hf$ ratios, indicating that the Hongshan F-rich granitic melt was not generated directly from these metamorphic rocks. One interpretation is that the source rocks for the parental magma of the Hongshan granites were basement metamorphic rocks significantly modified by juvenile mantle magmatism. Another possibility is that the

Hongshan granitic melt originated from crustal sources with a Mesoproterozoic model age, which have not been found in the studied area. The high SiO_2 contents and ASI index and low TFMM contents of the Hongshan granites argue against a strong influence of mantle-derived magmas. The lack of coeval mafic magmatism in the area provides further evidence against this interpretation. Therefore the Hongshan granitic melt most probably originated from Mesoproterozoic crustal material at depth. Although this kind of crustal component is not found in the area, it is exposed in the Lanhe area of northern Guangdong Province to the west (*Xu* et al., 2005).

Magma evolution

The high SiO_2 and low CaO and mafic components of the Hongshan granites suggest that the magma had undergone fractional crystallization in a deeper magma chamber before emplacement at its present level. The geochemical variations exhibited by the Hongshan granites (Figs. 3, 5) indicate that the magma experienced further fractional crystallization during emplacement and cooling. A decrease in mafic components (e.g. TFMM) and V and Co abundances may be the result of fractional crystallization of biotite and Fe–Ti oxides. Rb, Sr and Ba variations are mainly controlled by feldspars and biotite. Fractional crystallization modeling shows that the Sr and Ba depletion observed in the Hongshan granites can be explained by fractionation of K-feldspar or a combination of plagioclase and biotite (Fig. 10a). Considering the marked decrease in CaO/Na_2O, Eu/Eu^* and mafic components with declining temperature (Figs. 3, 5), the removal of plagioclase and biotite may be more important. Decreases in Zr, Hf, Th, REE and Y concentrations are consistent with the fractionation of some accessory minerals, especially zircon.

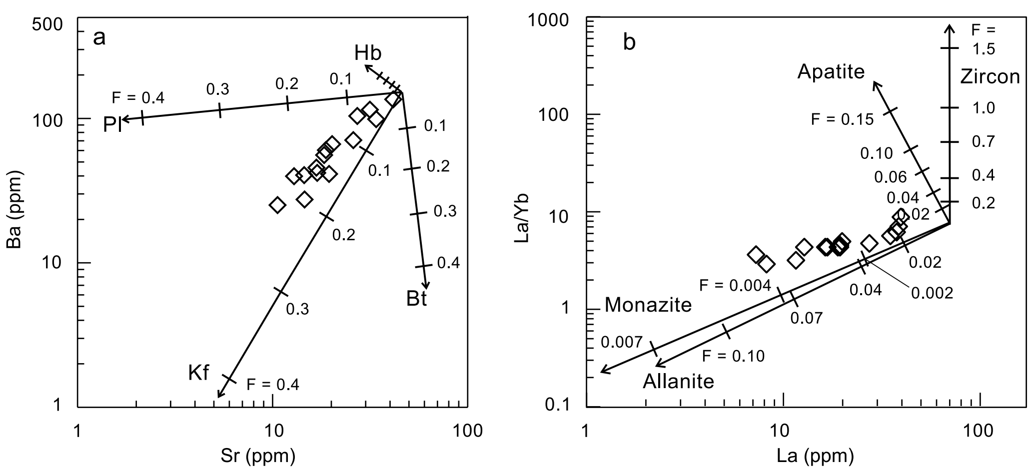

Fig. 10. Ba–Sr (**a**) and La–La/Yb (**b**) variation diagrams showing fractional crystallization of rock-forming mineral and accessory minerals of the Hongshan granites. In the Rayleigh fractionation model, Ba and Sr partitioning coefficients between rock-forming minerals and rhyolitic melt are from *Ewart* and *Griffin* (1994); La and Yb partitioning coefficients between accessory minerals and granitic melt are from *Bea* et al. (1994) and *Mahood* and *Hildreth* (1983). F in (**a**) and (**b**) refers to the extent of fractionation

Fractional crystallization modeling for REE indicates that the decrease in La content and La/Yb ratio may have been caused by minor fractionation of monazite or allanite (Fig. 10b). Monazite fractionation would also account for the decrease in Th concentration and Th/U. However, significant Zr and Hf depletion in more evolved samples must be related to zircon fractionation. In fact, zircon fractionation may compensate the decrease in La/Yb caused by removal of monazite, leading to the variation trend deviating from the calculated monazite fractionation line (Fig. 10b).

Strongly evolved F-rich peraluminous granites commonly experience two-stage evolution involving normal crystal fractionation followed by late-stage fluid fractionation (*Dostal* and *Chatterjee*, 1995; *Irber*, 1999). These granites have characteristic compositions including a strong lanthanide tetrad effect ($TE_{1,3} > 1.2$; *Irber*, 1999), low K/Rb (<50), Zr/Hf (<25) and Nb/Ta (<5) (*Dostal* and *Chatterjee*, 1995; *Shaw*, 1968; *Irber*, 1999), and Y/Ho ratios (>35 or <25) deviating significantly from the chondritic range (*Bau*, 1996; *Irber*, 1999). However, the Hongshan granites do not show a significant REE tetrad effect ($TE_{1,3} = 1.06$–1.19), and have relatively high K/Rb (>50) and Nb/Ta (mainly >5) and chondrite-like Y/Ho (27–30). These geochemical features suggest that the Hongshan granitic magma remained in the crystal fractionation stage, and did not reach a well-developed fluid fractionation stage, even though fluid fractionation may have become increasingly important during late-stage evolution.

On the other hand, previously described F-rich granitoids that underwent fluid fractionation processes generally formed in the last stages of magma evolution at shallow levels as small bodies or dykes of topaz quartzite and greisen (*Schwartz* and *Askury*, 1989; *Dostal* and *Chatterjee*, 1995; *Liu* et al., 1999; *Zhu* et al., 1993). They are commonly associated with rare-metal deposits, including Sn, W, and Nb–Ta. The Hongshan pluton is a relatively large granite body that was emplaced at relatively deep levels, as evidenced by the lack of acicular or fine-prismatic topaz grains and the absence of porphyritic textures with a fine-grained matrix, features which would reflect a rapidly cooling environment (*Liu* et al., 1999). So far, no Sn, W and Nb mineralization related to the Hongshan granites has been found, consistent with the other evidence that the studied samples are not the products of a magma that experienced obvious fluid fractionation.

Although the studied samples are not the products of strongly evolved magmas, it cannot be excluded that there are strongly evolved greisens or granitoid veins associated with rare metal mineralization within the pluton or near the contact zone with wall-rocks. Therefore some geochemical parameters of the Hongshan granites have been plotted with sampling locations to inspect their spatial variation and determine the region with the highest potential for mineralization. Some geochemical parameters, including Sn, W, REE, Zr, Th, and Rb exhibit a weak spatial zonation (Fig. 11), with the most evolved samples located in the southeastern part of the pluton. Hence, if there are rare-metal deposits associated with the Hongshan granite, the most likely target is in this southeastern region, with longitude and latitude between 116°8′E–116°10′E and 25°29′N–25°32′N.

The Hongshan granites also exhibit significant Sm–Nd isotopic variation with progressive magma evolution (Table 4, Fig. 8), which is best accounted for by the assimilation of wall-rocks during fractional crystallization after emplacement.

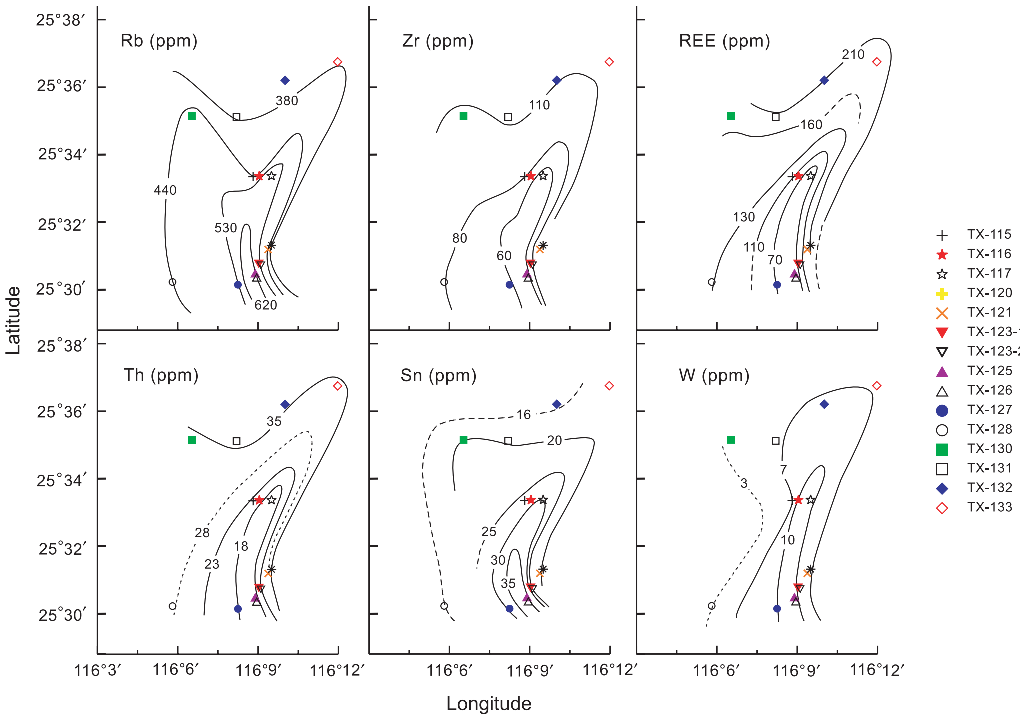

Fig. 11. Spatial variations of some trace elements in the Hongshan granites

The abundant volatile components of the magma and wall-rocks (mica schist and gneiss) are prone to compositional exchange between them. Sample TX-121 is a less evolved sample with highest εNd(225) (−7.9), similar within uncertainties to the εNd(225) value (−6.5) calculated using its zircon Hf-isotope compositions and the equation proposed by *Vervoort* et al. (1999). The small difference is consistent with zircon being an earlier-crystallizing phase; the isotopic composition of the zircon may represent that of the relatively primary magma with little assimilation of wall-rocks. If the parental Hongshan melts were contaminated by the Taoxi Group metamorphic wall-rocks, Sm–Nd isotopic variation of the Hongshan granites can be modeled as the results of an assimilation and fractional crystallization (AFC) process as shown in Fig. 8. In AFC modeling, the average value of nine Taoxi Group metamorphic wall-rocks is regarded as the composition (C_a) of the assimilated material, i.e. C_a (Sm) = 7.0, C_a (Nd) = 36 and $^{143}Nd/^{144}Nd_a^0 = 0.51170$ (Table 2; *Shen* et al., 2003). The original magma compositions (C_m) are assumed to be C_m^0 (Sm) = 8.8, C_m^0 (Nd) = 43 and $^{143}Nd/^{144}Nd_m^0 = 0.51197$, extrapolated from the elemental and isotope variation trends (Fig. 8). Bulk partition coefficients for Sm and Nd are assumed to be $D_{Sm} = 1.7$ and $D_{Nd} = 2.4$, according to decrease in Sm and Nd contents and Nd/Sm ratio during magmatic evolution. AFC calculation equation is after *DePaolo* (1981), where r = 0.85. The modeling results show that the AFC process can produce the Sm–Nd isotopic variation (expressed as εNd(225) and Sm/Nd) of the Hongshan granites (Fig. 8a). Therefore, in some cases the Sm–Nd isotopic compositions does not reflect the features of the original melt and its source, especially in fluid-rich magmas with slow cooling rates (e.g. at depth). Thus the Hf-isotope compositions of the zircons may be more representative of the original source rock as demonstrated by this study.

Tectonic setting of magma generation

Strongly peraluminous or S-type granites are generally thought to occur in synorogenic environments (*Pearce* et al., 1984; *Harris* et al., 1986). Many workers have attributed the formation, segregation and emplacement of these granitic melts to compressional regimes (*Brown* and *Solar*, 1998; *Muzio* and *Artur*, 1999; *Brown*, 2001; *Atherton* and *Ghani*, 2002; *Sheppard* et al., 2003). However, some recent studies suggest that this type of granite also occurs in extensional settings (*Turner* et al., 1992; *Pearce*, 1996; *Searle* et al., 1997; *Sylvester*, 1998; *Healy* et al., 2004, *Chen* et al., 2002).

The Hongshan granite pluton formed in early Mesozoic (Indosinian) time. Many other Indosinian granites are distributed sporadically within the Nanling belt and neighboring areas (Fig. 1). *Zhou* (2003), *Sun* et al. (2005) and *Ling* et al. (2005) argued that these granites formed in an extensional setting following the peak collision between the Sibumasu and Indo-China blocks, analogous to strongly peraluminous granites in the Hercynian and Himalaya orogens. However, the Hercynian orogen contains numerous post-collisional mafic rocks and high-K calc-alkaline granitoids (*Rottura* et al., 1998; *Sylvester*, 1998), whereas the Himalaya orogen developed widespread potassium-rich lavas and sodium-rich basalts from 50 to 30 Ma, and ultrapotassic and adakitic lavas between ~26 and 10 Ma (*Chung* et al., 2005). In the SE China block, >95% of the Indosinian igneous rocks are granites, of which more than 93 vol.% are peraluminous (*Sun* et al., 2005), but mafic and alkaline volcanic rocks and calc-alkaline granitoids, as well as high-grade metamorphic rocks, are absent. On the other hand, no Indosinian orogenic belt parallel to the collision zone between Sibumasu and Indo-China can be distinguished in the SCB. Therefore Indosinian granites in SE China probably did not form in a collapse setting during relaxation of crust thickened by collision as in the Hercynian and Himalayan orogens.

In fact, the Hongshan granite and other Indosinian granites in SE China formed almost simultaneously with both the collision between the North China Block (NCB) and the South China Block (SCB) along the Qingling-Dabieshan-Sulu ultrahigh-pressure metamorphic belt (*Rowley* et al., 1997; *Zheng* et al., 2004) and the accretion of the Sibumasu block to the Indochina-SCB block in Middle Triassic (*Carter* et al., 2001). The integrated Indochina-SCB block underwent clockwise rotation during the Middle Triassic collision (*Carter* et al., 2001), while the Indochina peninsula extruded southeastward along the Red River fault and rotated clockwise in the late Oligocene (*Zhou* et al., 1995; *Wang* et al., 1998). Therefore, the present NW–SE trending collisional belt should originally have been oriented E–W or NWW. Thus, the SCB was clamped between these two collision belts, resulting in a significant compressional stress. In this period, strong folding, thrust faulting and nappe structures were developed in the SCB (*Shu* et al., 1994; *Zhu* et al., 1999; *Zhang* and *Zhu*, 2003; *Liang* et al., 2005). The absence of synchronous bimodal volcanic rocks or A-type granitoids also supports a collisonal rather than extensional setting. Consequently, the Hongshan granite and other early Mesozoic (Indosinian) granites may have formed in a compressional tectonic environment. However, these granites (generally not showing any directional fabric) occur throughout the central and southwestern SCB (Fig. 1), and are not concentrated along an orogenic belt. Therefore, the generation of Indosinian granitic melts in the inner SCB may have been controlled by strike-slip faults triggered by collision. In fact, most Indosinian granites are now generally distributed along NEE and NNW trends, interpreted as conjugate strike-slip faults, and are especially concentrated at the intersection of two faults (Fig. 1).

Conclusions

LAM-ICPMS U–Pb zircon dating indicates that the Hongshan granites formed at ca. 225 Ma. U–Pb dating results for two large monazite grains and inherited zircons with different Hf-isotope composition and internal structure show that the area underwent several thermal events from ~280 to 240 Ma. Strongly peraluminous (ASI > 1.1) geochemical characteristics and low Hf-isotope ratios of the main zircon population indicate that the original melt of the Hongshan granites was probably generated from lower crustal sedimentary rocks of Mesoproterozoic age.

The variations in element concentrations and ratios and $^{143}Nd/^{144}Nd$ ratios in the Hongshan granites indicate that the magma underwent strong fractional crystallization involving the removal of feldspar, biotite and accessory minerals, such as monazite and zircon, but did not reach a highly evolved fluid-rich stage commonly seen in mineralized topaz-bearing granites worldwide. If there is mineralization associated with the Hongshan granite it would probably be located in the southeastern part of the intrusion where geochemical parameters indicate the maximum fractionation and the most fluid-rich late-stage evolution occurs in this body.

Variations in $^{143}Nd/^{144}Nd$ and $^{147}Sm/^{144}Nd$ during magma evolution reflect AFC interaction with the Taoxi Group wall rocks during emplacement and cooling, whereas Hf isotope compositions of zircons from less-evolved samples more reliably reveal the nature of the original magma. Thus, the *in situ* U–Pb dating of zircon along with Hf-isotope analyses of the same zones in the zircons is shown by this study to be a powerful tool to track changes in the composition of such magmas through their crystallization, assimilation or magma mixing and to assess source components and the crystallization age of granitic bodies.

The Hongshan granite and other Indosinian granites in the SCB were produced in a syn-orogenic tectonic setting; magma emplacement probably was controlled by strike-slip faults that were triggered by compression. Deep faults not only allowed ascent of mantle fluids, decompression at deep levels and the partial melting of lower crust, but also provided the space for melt emplacement.

Acknowledgements

We thank Norman Pearson and Suzie Elhlou for expert and cheerful assistance with zircon analytical work at GEMOC. We also thank Qi Liang for her expert ICPMS support. Chen

Zelin, Zhuang Jianmin and Xie Lei are thanked for their assistance in field work and sample collection. This work was supported by the NSF of China Grants (No. 40221301, 40372087 and 40132010) and ARC Discovery and Linkage International grants (S. Y. O'Reilly and W. L. Griffin). This work used instrumentation funded by ARC LIEF and DEST Systemic Infrastructure Grants and Macquarie University. Constructive and detailed reviews by Dr. Wolfgang Siebel and Dr. Urs Kloetzli significantly improved the manuscript. This is Contribution 448 from the National Key Centre for Geochemical Evolution and Metallogeny of Continents (www.es.mq.edu.au/GEMOC/).

References

Andersen T (2002) Correction of common lead in U–Pb analyses that do not report ^{204}Pb. Chem Geol 192: 59–79

Atherton MP, Ghani AA (2002) Slab breakoff: a model for Caledonian, late granite syn-collisional magmatism in the orthotectonic (metamorphic) zone of Scotland and Donegal, Ireland. Lithos 62: 65–85

Bau M (1996) Controls on the fractionation of isovalent trace elements in magmatic and aqueous systems: evidence from Y/Ho, Zr/Hf, and lanthanide tetrad effect. Contrib Mineral Petrol 123: 323–333

Bea F, Pereira MD, Stroh A (1994) Mineral/leucosome trace-element partitioning in a peraluminous migmatite (a laser ablation-ICP-MS study). Chem Geol 117: 291–312

Boynton WV (1984) Geochemistry of the rare earth elements: meteorite studies. In: *Hendeerson P* (ed) Rare earth element geochemistry. Netherlands: Elservier, pp 63–114

Brown M (2001) Crustal melting and granite magmatism: Key issues. Phys Chem Earth (A) 26: 201–212

Brown M, Solar GS (1998) Granite ascent and emplacement during contractional deformation in convergent orogens. J Strut Geol 20: 1365–1393

Carter A, Roques D, Bristow C, Kinny P (2001) Understanding Mesozoic accretion in Southeast Asia: Significance of Triassic thermotectonism (Indosinian orogeny) in Vietnam. Geology 29: 211–214

Chen P, Kong X, Wang Y, Ni Q, Zhang B, Ling H (1999) Rb–Sr isotopic dating and significance of early Yanshanian bimodal volcanic-intrusive complex from south Jiangxi Province. Geol J China Univ 5: 378–383 (in Chinese)

Chen P, Hua R, Zhang B, Lu J, Fan C (2002) Early Yanshanian post-orogenic granitoids in the Nanling region – Petrological constraints and geodynamic settings. Sci China (D) 45: 755–768

Chen PR, Zhou XM, Zhang W, Li H, Fan C, Sun T, Chen W, Zhang M (2005) Petrogenesis and significance of early Yanshanian syenite-granite complex in eastern Nanling Range. Sci China (D) 48: 912–924

Christiansen EH, Burt DM, Sheridan MF, Wilson RT (1983) The petrogenesis of topaz rhyolites from the Western United States. Contrib Mineral Petrol 83: 16–30

Chung SL, Chu MF, Zhang Y, Xie Y, Lo CH, Lee TY, Lan CY, Li X, Zhang Q, Wang Y (2005) Tibetan tectonic evolution inferred from spatial and temporal variations in post-collisional magmatism. Earth Sci Rev 68: 173–196

Deer WA, Howie RA, Zussman J (1966) An introduction to the rock-forming minerals. Longmans, London, pp 696

Deniel C, Vidal P, Fernandez A (1987) Isotopic study of the Manaslu granite (Himalaya, Nepal): inferences on the age and source of Himalayan leucogranites. Contrib Mineral Petrol 96: 78–92

DePaolo DJ (1981) Trace element and isotopic effects of combined wallrock assimilation and fractional crystallization. Earth Plant Sci Lett 53: 189–202

Ding X, Chen P, Chen W, Huang H, Zhou X (2006) Single zircon LA-ICPMS U–Pb dating of Weishan granite (Hunan, South China) and its petrogenetic significance. Sci China (D) 49: 816–827

Dostal J, Chatterjee AK (1995) Origin of topaz-bearing and related peraluminous granites of the late Devonian Davis Lake pluton, Nova Scotia, Canada: crystal versus fluid fractionation. Chem Geol 123: 67–88

Du S-H, Huang Y-H (1984) Xianghualingite – A new type of magmatic rocks. Sci China (B) 11: 1039–1049 (in Chinese)

Ewart A, Griffin WL (1994) Application of proton-microprobe data to trace-element partitioning in volcanic rocks. Chem Geol 117: 251–284

Foord EE, Jackson LL, Taggart JE (1992) Environment of crystallization of topaz as inferred from crystal chemistry and infrared spectra. In: *Francis CA* (ed) Rochester Mineralogical Symposium, Eighteenth technical session. Heldref Publications, Washington DC, United States, pp 112–113

Frindta S, Trumbull RB, Romer RL (2004) Petrogenesis of the Gross Spitzkoppe topaz granite, central western Namibia: a geochemical and Nd-Sr-Pb isotope study. Chem Geol 206: 43–71

Griffin WL, Wang X, Jackson SE, Pearson NJ, O'Reilly SY, Xu X, Zhou X (2002) Zircon chemistry and magma mixing, SE China: In-situ analysis of Hf isotopes, Tonglu and Pingtan igneous complexes. Lithos 61: 237–269

Harris NBW, Pearce JA, Tindle AG (1986) Geochemical characteristics of collision zone magmatism. In: *Coward MP*, *Reis AC* (eds) Collision tectonics. Spec Public Geol Soc, London, 19: 67–81

Healy B, Collins WJ, Richards SW (2004) A hybrid origin for Lachlan S-type granites: the Murrumbidgee batholith example. Lithos 78: 197–216

Henderson CMB, Martin JS, Mason RA (1989) Compositional relations in Li-micas from SW England and France: An ion- and electron microprobe study. Mineral Mag 53: 427–449

Henry DJ, Guidotti CV (1985) Tourmaline as petrogenetic indicator minerals: an example from staurolite-grade metapelites of NW Maine. Am Mineral 70: 1–15

Hu GR, Zhang BT (1998) Neodymium isotope composition and source materials of the metabasement in central Jiangxi province. Acta Petrol Mineral 17: 35–39 (in Chinese)

Irber W (1999) The lanthanide tetrad effect and its correlation with K/Rb, Eu/Eu*, Sr/Eu, Y/Ho, and Zr/Hf of evolving peraluminous granite suites. Geochim Cosmochim Acta 63: 489–508

Jackson SE, Pearson NJ, Griffin WL, Belousova EA (2004) The application of laser ablation-inductively coupled plasma-mass spectrometry to in-situ U–Pb zircon geochronology. Chem Geol 211: 47–69

Kesraoui M, Nedjari S (2002) Contrasting evolution of low-P rare metal granites from two different terranes in the Hoggar area, Algeria. J Afr Earth Sci 34: 247–257

Krogstad EJ, Walker RJ (1996) Evidence of heterogeneous crustal source: the Harney Peak granite, South Dakota, USA. Royal Soc Edinburgh, Earth Sci 87: 331–337

Lapierre H, Jahn BM, Charvet J, Yu YW (1997) Mesozoic felsic arc magmatism and continental olivine tholeiites in Zhejiang Province and their relationship with the tectonic activity in southeastern China. Tectonophysics 274: 321–338

Lenharo SLR, Pollard PJ, Born H (2003) Petrology and textural evolution of granites associated with tin and rare-metals mineralization at the Pitinga mine, Amazonas, Brazil. Lithos 66: 37–61

Li X, Zhou H, Liu Y, Li J, Sun M, Chen Z (2000) Shoshonitic intrusive suite in SE Guangxi: petrology and geochemistry. Chin Sci Bull 45: 653–658

Li X, Chen Z, Liu D, Li W (2003) Jurassic gabbro-granite-syenite suites from Southern Jiangxi Province, SE China: age, origin, and tectonic significance. Inter Geol Rev 45: 898–921

Li X-H, Li Z-X, Li W-X, Wang Y (2006) Initiation of the Indosinian orogeny in South China: evidence for a Permian magmatic arc on Hainan Island. J Geol 114: 341–353

Liang X, Li X, Qiu Y, Yang D (2005) Indosinian collisional orogeny: evidence from structural and sedimentary geology in Shiwandashan Basin, South China. Geotect Metal 29: 99–112 (in Chinese)

Ling H, Shen W, Deng P, Jiang S, Jiang Y, Qiu J, Huang G, Ye H, Tan Z (2005) Study of geochemistry and petrogenesis of the Maofeng granite, northern Guangdong province. Acta Petrol Sin 21: 677–687 (in Chinese)

Liu CS, He B (1991) A preliminary discussion on the genesis of topaz-bearing magmatic rocks in Southeastern Jiangxi province. J Nanjing Univ (Earth Sci) 3: 220–230 (in Chinese)

Liu CS, Ling HF, Hong XL (1999) An F-rich, Sn-bearing volcanic-intrusive complex in Yanbei, South China. Econ Geol 94: 325–342

Liu CS, Shen W, Wang D (1995) The characteristics and genetic mechanism of igneous topazites in South China. Acta Geol Sin 69: 221–231 (in Chinese)

London D (1992) Phosphorus in S-type magmas: the P_2O_5 content of feldspars from peraluminous granites, pegmatite and rhyolite. Am Mineral 77: 126–145

Ludwig KR (2001) Users manual for Isoplot/Ex, rev. 2.49, a geochronological toolkit for Microsoft Excel. Berkeley Geochronology Center, Spec Public 1a: 58 pp

Mahood G, Hildreth W (1983) Large partition coefficients for trace elements in high-silica rhyolites. Geochim Cosmochim Acta 47: 11–30

Manning DAC, Hill PI (1990) The petrogenetic and metallogenetic significance of topaz granite from the S.W. England orefield. Geol Soc Am Spec Pap 246: 51–69

Muzio R, Artur AC (1999) Petrological of the Santa Teresa granitic complex southeastern Uruguay. J South Am Earth Sci 12: 501–510

Pearce JA (1996) Sources and settings of granitic rocks. Episodes 19: 120–125

Pearce JA, Harris NBW, Tindle AG (1984) Trace element discrimination diagrams for the tectonic interpretation of granitic rocks. J Petrol 25: 956–983

Qi L, Gregoire DC (2000) Determination of trace elements in twenty-six Chinese geochemistry reference materials by Inductively Coupled Plasma-Mass Spectrometry. Geostand Newlett 24: 51–63

Qiu J, Hu J, Wang X, Jiang S, Wang R, Xu X (2005) The Baishigang pluton in Heyuan, Guangdong Province: a highly fractionated I-type granite. Acta Geol Sin 79: 503–514 (in Chinese)

RGSTFJ: Regional Geology Survey Team of Fujian Province (2000) The 1:50000 regional geologic mapping of Taoxi, Sidu, Yongping and Tufang area, Fujian, pp 1–149 (in Chinese)

RGSTJX: Regional Geology Survey Team of Jiangxi Province (1991) The 1:50000 geologic mapping of Huichang in Jiangxi province. China University of Geology Press, Wuhan, pp 1–120 (in Chinese)

Rottura A, Bargossi GM, Caggianelli A, Del Moro A, Visona D, Tranne CA (1998) Origin and significance of the Permian high-K calc-alkaline magmatism in the central-eastern Southern Alps, Italy. Lithos 45: 329–348

Rowley DB, Xue F, Tucker RD, Peng ZX, Baker J, Davis A (1997) Ages of ultrahigh pressure metamorphism and protolith orthogneisses from the eastern Dabie Shan: U/Pb zircon geochronology. Earth Planet Sci Lett 151: 191–203

Schwartz MO, Askury AK (1989) Geologic, geochemical, and fluid inclusion studies of the tin granites from the Bujang Melaka pluton, Kinta Valley, Malaysia. Econ Geol 84: 751–779

Searle MP, Parrish RR, Hodges KV, Hurfold A, Ayres MW, Whitehouse MJ (1997) Shisha Pangma leucogranite, South Tibetan Himalaya: field relations, geochemistry, age, origin, and emplacement. J Geol 105: 295–317

Shaw DM (1968) A review of K–Rb fractionation trends by covariance analysis. Geochim Cosmochim Acta 32: 573–176

Shen W, Ling H, Li W, Wang D, Huang X, Pan J (1999) The Nd–Sr isotope study of Mesozoic granitoids in Jiangxi Province. Chin Sci Bull 44: 1427–1431

Shen W, Yu J-H, Zhao L, Chen Z, Lin H (2003) Nd isotopic characteristics of post-Archean sediments from the Eastern Nanling Range: Evidence for crustal evolution. Chin Sci Bull 48: 1679–1685

Sheppard S, Occhipinti SA, Tyler IM (2003) The relationship between tectonism and composition of granitoid magmas, Yarlarweelor gneiss complex, western Australia. Lithos 66: 133–154

Shu L, Guo L, Shi Y, Sun Y (1994) Kinematic study on the southern marginal fault zone of the Jiuling Mountains, Jiangxi Province. Sci Geol Sin 29: 209–219 (in Chinese)

Sun T, Zhou X, Chen P, Li H, Zhou H, Wang Z, Shen W (2005) Strongly peraluminous granites of Mesozoic in Eastern Nanling Range, southern China: Petrogenesis and implications for tectonics. Sci China (D) 48: 165–174

Sylvester PJ (1998) Post-collisional strongly peraluminous granites. Lithos 45: 29–44

Taylor RP (1992) Petrological and geochemical characteristics of the Pleasant Ridge zinnwaldite-topaz granite, southern New Brunswick and comparisons with other topaz-bearing felsic rocks. Can Mineral 30: 895–921

Taylor SR, McLennan SM (1985) The continental crust: its composition and evolution. Blackwell, Oxford, pp 312

Tischendorf G, Gottesmann B, Förster HJ, Trumbull RB (1997) On Li-bearing micas: Estimating Li from electron microprobe analyses and an improved diagram for graphical representation. Mineral Mag 61: 809–834

Turner S, Sandiford M, Foden J (1992) Some geodynamic and compositional constraints on ''postorogenic''; magmatism. Geology 20: 931–934

Vervoort JD, Patchett PJ, Blichert-Toft J, Albarede F (1999) Relationships between Lu–Hf and Sm–Nd isotopic systems in the global sedimentary system. Earth Planet Sci Lett 168: 79–99

Wang D, Liu C, Shen W, Min M, Ling H (1994) Geochemical characteristics and genesis of topaz-bearing porphyries in Yangbin area of Taishun country, Zhejiang. Geochimica 23: 115–124 (in Chinese)

Wang P-L, Lo C-H, Lee T-Y, Chung S-L, Lan C-Y, Yem NT (1998) Thermo-chronological evidence for the movement of the Ailao Shan-Red River shear zone: A perspective from Vietnam. Geology 26: 887–890

Watson EB, Harrison TM (1983) Zircon saturation revisited: temperature and composition effects in a variety of crustal magma types. Earth Planet Sci Lett 64: 295–301

Whalen JB, Currie KL, Chappell BW (1987) A-type granites: geochemical characteristics, discrimination and petrogenesis. Contrib Mineral Petrol 95: 406–419

Xie D, Ma R, Zhang Y, Zhao X, Coe RS (1996) Crust growth and mantle plume tectonics of South China continent. Geological Publishing House, Beijing (in Chinese)

Xiong XL, Rao B, Chen FR, Zhu J, Zhao Z (2002) Crystallization and melting experiments of a fluorine-rich leucogranite from the Xianghualing pluton, South China, at 150 MPa and H_2O-saturated conditions. J Asian Earth Sci 21: 175–188

Xu X, Dong C, Li W, Zhou X (1999) Late Mesozoic intrusive complexes in the coastal area of Fujian, SE China: the significance of the gabbro-diorite-granite association. Lithos 46: 299–315

Xu X, O'Reilly SY, Griffin WL, Deng P, Pearson NJ (2005) Relict Proterozoic basement in the Nanling Mountains (SE China) and its tectonothermal overprinting. Tectonics 24: TC2003, doi: 10.1029/2004 TC001652

Yu J-H, Zhou X, Zhao L, Chen X (2003) Discovery and implications of granulite facies metamorphic rocks in the eastern Nanling, China. Acta Petrol Sin 19: 461–467 (in Chinese)

Yu J-H, Zhou X, O'Reilly YS, Zhao L, Griffin WL, Wang R, Wang L, Chen X (2005) Formation history and protolith characteristics of granulite facies metamorphic rock in Central Cathaysia deduced from U–Pb and Lu–Hf isotopic studies of single zircon grains. Chin Sci Bull 50: 2080–2089

Yu J-H, O'Reilly YS, Wang L, Griffin WL, Jiang S, Wang R, Xu X (2006) Finding of ancient materials in Cathaysia and implication for the formation of Precambrian crust. Chin Sci Bull 51: (in press)

Zhang KJ, Zhu JX (2003) Intracontinental deformation of South China due to penetration of North China: fold and thrust structures and their ore-controlling in southern Anhui, South China. J Nanjing Univ (Natural Sci) 39: 746–753 (in Chinese)

Zhao L, Yu J-H, Xie L (2004) Geochemistry and origin of the Hongshan topaz-bearing leucogranites in southwestern Fujian Province. Geochimica 33: 372–386 (in Chinese)

Zheng Y-F, Wu Y-B, Chen F, Gong B, Li L, Zhao Z-F (2004) Zircon U–Pb and oxygen isotope evidence for a large-scale ^{18}O depletion event in igneous rocks during the Neoproterozoic. Geochim Cosmochim Acta 68: 4145–4165

Zhou D, Ru K, Chen H (1995) Kinematics of Cenozoic extension on the South China Sea continental margin and its implications for the tectonic evolution of the region. Tectonophysics 251: 161–177

Zhou X (2003) My thinking about granite genesis of South China. Geol J China Univ 9: 556–565 (in Chinese)

Zhou XM, Li, WX (2000) Origin of Late Mesozoic igneous rocks in SE China: implications for lithosphere subduction and underplating of mafic magma. Tectonophysics 326: 269–287

Zhu D, Meng X, Peng S, Feng X, Wang J (1999) Primary study on the western Guangdong nappe zone in the Hercynian and Indosinian Epoch. J Geomech 5: 51–58 (in Chinese)

Zhu JC, Liu WX, Zhou F (1993) Ongonite and topazite in dike No. 431 of Xianghualing district and their spatial zonation and genetic relationship. Acta Petrol Sin 9: 158–166 (in Chinese)

Authors' addresses: *Jin-Hai Yu* (corresponding author; e-mail: jhyu@nju.edu.cn), *Lei Zhao* (e-mail: zhaolei@nju.org.cn), *Xinmin Zhou* (e-mail: xuezhou@nju.edu.cn), *Shaoyong Jiang* (e-mail: shyjiang@public1.ptt.js.cn), *Lijuan Wang* (e-mail: wanglijuan665@sohu.com) and *Rucheng Wang* (e-mail: rcwang@nju.edu.cn), State Key Laboratory for Crust-Mantle Evolution and Deposit Research, Department of Earth Sciences, Nanjing University, Nanjing 210093, P.R. China; *Suzanne Y. O'Reilly* (e-mail: sue.oreilly@mq.edu.au), *William L. Griffin* (e-mail: bill.griffin@mq.edu.au), *Ming Zhang* (e-mail: ming.zhang@mq.edu.au), GEMOC ARC National Key Centre, Department of Earth and Planetary Sciences, Macquarie University, Sydney, N.S.W. 2109, Australia

Verleger: Springer-Verlag GmbH, Sachsenplatz 4–6, 1201 Wien, Austria – Herausgeber: Prof. Dr. J. G. Raith, Department Angewandte Geowissenschaften und Geophysik, Lehrstuhl für Mineralogie und Petrologie, Peter-Tunner-Straße 5, 8700 Leoben, Austria – Redaktion: Peter-Tunner-Straße 5, 8700 Leoben, Austria – Hersteller: Satz und Umbruch: Thomson Press (India) Ltd., Chennai; Offsetdruck: Krips bv, Kaapweg 6, 7944 HV Meppel, The Netherlands – Verlagsort: Wien – Herstellungsort: Meppel – Printed in The Netherlands.